Yeast Vps13 promotes mitochondrial function and is localized at membrane contact sites

Jae-Sook Park[a], Mary K. Thorsness[b], Robert Policastro[a], Luke L. McGoldrick[a], Nancy M. Hollingsworth[a], Peter E. Thorsness[b], and Aaron M. Neiman[a,*]
[a]Department of Biochemistry and Cell Biology, Stony Brook University, Stony Brook, NY 11794-5215; [b]Department of Molecular Biology, University of Wyoming, Laramie, WY 82071

ABSTRACT **The Vps13 protein family is highly conserved in eukaryotic cells. Mutations in human *VPS13* genes result in a variety of diseases, such as chorea acanthocytosis (ChAc), but the cellular functions of Vps13 proteins are not well defined. In yeast, there is a single *VPS13* orthologue, which is required for at least two different processes: protein sorting to the vacuole and sporulation. This study demonstrates that *VPS13* is also important for mitochondrial integrity. In addition to preventing transfer of DNA from the mitochondrion to the nucleus, *VPS13* suppresses mitophagy and functions in parallel with the endoplasmic reticulum–mitochondrion encounter structure (ERMES). In different growth conditions, Vps13 localizes to endosome–mitochondrion contacts and to the nuclear–vacuole junctions, indicating that Vps13 may function at membrane contact sites. The ability of *VPS13* to compensate for the absence of ERMES correlates with its intracellular distribution. We propose that Vps13 is present at multiple membrane contact sites and that separation-of-function mutants are due to loss of Vps13 at specific junctions. Introduction of *VPS13A* mutations identified in ChAc patients at cognate sites in yeast *VPS13* are specifically defective in compensating for the lack of ERMES, suggesting that mitochondrial dysfunction might be the basis for ChAc.**

Monitoring Editor
Sandra Lemmon
University of Miami

Received: Feb 18, 2016
Revised: Jun 3, 2016
Accepted: Jun 3, 2016

INTRODUCTION

Yeast *VPS13* is the founding member of a highly conserved gene family found in all eukaryotes. In humans, there are four *VPS13* orthologues: *VPS13A*, *B*, *C*, and *D* (Velayos-Baeza *et al.*, 2004). Mutations in *VPS13A*, *B*, and *C* are associated with the neurodegenerative disorder chorea acanthocytosis (ChAc), the developmental disorder Cohen syndrome, and Parkinson's disease, respectively (Ueno *et al.*, 2001; Kolehmainen *et al.*, 2003; Lesage *et al.*, 2016). Despite the importance and conservation of this family, the functions of the different Vps13 family proteins are elusive.

Most of our knowledge of *VPS13* function comes from studies in *Saccharomyces cerevisiae*, in which there is just a single version of the gene. *VPS13* was originally identified by a mutant that is defective in sorting the vacuolar protease carboxypeptidase Y (CPY) to the vacuole, resulting in secretion of CPY protein (Bankaitis *et al.*, 1986). This sorting defect is due to a failure to transport the sorting receptor for CPY from the endosome to the Golgi (Brickner and Fuller, 1997). *VPS13* is also required for the process of sporulation, which is independent of its function in vacuolar sorting (Brickner and Fuller, 1997; Enyenihi and Saunders, 2003; Nakanishi *et al.*, 2007; Park and Neiman, 2012). A critical step in spore formation is the de novo synthesis of prospore membranes that encapsulate the haploid products of meiosis (Neiman, 2011; Park and Neiman, 2012). *VPS13* is essential for prospore membrane formation, in which it promotes the presence of the lipids phosphatidylinositol (PtdIns)-4-phosphate and PtdIns-4,5-bisphosphate. This function appears to be conserved, as a reduction in PtdIns-4-phosphate levels at plasma membranes was also observed when *VPS13A* was knocked down by RNA interference in mammalian cell lines (Park and Neiman, 2012; Park *et al.*, 2015). These results implicate *VPS13* in some aspect of lipid metabolism, although whether *VPS13* directly affects lipid

This article was published online ahead of print in MBoC in Press (http://www.molbiolcell.org/cgi/doi/10.1091/mbc.E16-02-0112) on June 8, 2016.

*Address correspondence to: Aaron M. Neiman (Aaron.neiman@stonybrook.edu).

Abbreviations used: ChAc, chorea acanthocytosis; CPY, carboxypeptidase Y; ERMES, ER-mitochondrion encounter site; mtDNA, mitochondrion DNA; YPA, yeast extract/peptone/acetate.

phosphorylation or influences the levels of these lipids through a more indirect mechanism is not known.

Membrane contact sites are created where membranes from two different organelles form stable junctions (Helle *et al.*, 2013). These sites may mediate transfer of lipids and ions between organelles (Henne *et al.*, 2015; Olkkonen, 2015; Raiborg *et al.*, 2015; Schrader *et al.*, 2015). Many different protein complexes have been defined at membrane contact sites, which generally consist of 1) structural proteins that serve to link the membranes together and 2) transfer proteins that are recruited to the contact site to mediate exchange of material. Different contact sites can be functionally linked so that sites between one pair of organelles respond to changes in sites between a different pair of organelles (Elbaz-Alon *et al.*, 2014, 2015). For instance, when subunits of the endoplasmic reticulum (ER)–mitochondrion contact site ERMES are mutated, a vacuolar–mitochondrial contact site called vCLAMP expands (Elbaz-Alon *et al.*, 2014; Honscher *et al.*, 2014). The combination of mutants in both ERMES and vCLAMP subunits is lethal, supporting the idea that the vCLAMP contact site expansion occurs to compensate for the loss of ERMES (Elbaz-Alon *et al.*, 2014; Honscher *et al.*, 2014).

The ERMES complex comprises the integral ER membrane protein Mmm1, the outer mitochondrial membrane proteins Mdm10 and Mdm34, and the soluble protein Mdm12 (Kornmann and Walter, 2010). Disruption of the genes encoding these proteins causes the loss of ERMES contact sites. Mutants deleted for *MMM1* are viable but grow slowly. They rapidly lose mitochondrial DNA and cannot grow on nonfermentable carbon sources such as glycerol (Hobbs *et al.*, 2001; Hanekamp *et al.*, 2002). Deletion of *VPS13* is synthetically lethal in combination with mutants in different subunits of the ERMES complex, including *mmm1Δ* (Costanzo *et al.*, 2010; Hoppins *et al.*, 2011; Lang *et al.*, 2015). The requirement for *VPS13* in the absence of ERMES suggests a third, distinct role for *VPS13* in mitochondrial homeostasis, as well as a connection between *VPS13* and membrane contact sites.

This study reports that the *vps13Δ* mutants display mitochondrial defects, identifying a role for *VPS13* in mitochondrial homeostasis. Separation-of-function alleles were identified that affect both the function and localization of the protein. Altering the distribution of Vps13 results in different phenotypes, suggesting a model in which *VPS13* functions at multiple membrane contact sites to promote different cellular processes. In addition, mutations found in ChAc patients, when introduced into the yeast *VPS13*, result in specific loss of the mitochondrial homeostasis function of *VPS13*, suggesting that the neurodegenerative symptoms of ChAc could be due to mitochondrial dysfunction.

RESULTS

VPS13 is important for mitochondrial integrity

Defects in mitochondrial integrity can be detected using an assay for mutants that exhibit an increased frequency of transfer of mitochondrial DNA (mtDNA) from the mitochondrion to the nucleus (defined as "mitochondrial escape"; Thorsness and Fox, 1993). The mitochondrial escape assay uses a strain in which the *TRP1* gene is deleted from its chromosomal locus in the nucleus and inserted instead into the mitochondrial genome, rendering the cells auxotrophic for tryptophan. Transfer of the *TRP1* gene from the mitochondrion to the nucleus allows appropriate expression, resulting in growth on medium lacking tryptophan. The *MMM1* gene was previously identified by this screen (Hanekamp *et al.*, 2002). An allele of *VPS13*, *vps13-31* (previously *yme3-1*), showed high levels of Trp^+ papillae in this assay, indicating a loss in mitochondrial integrity (Figure 1A). The *vps13-31* mutation is a deletion of base pair 1565,

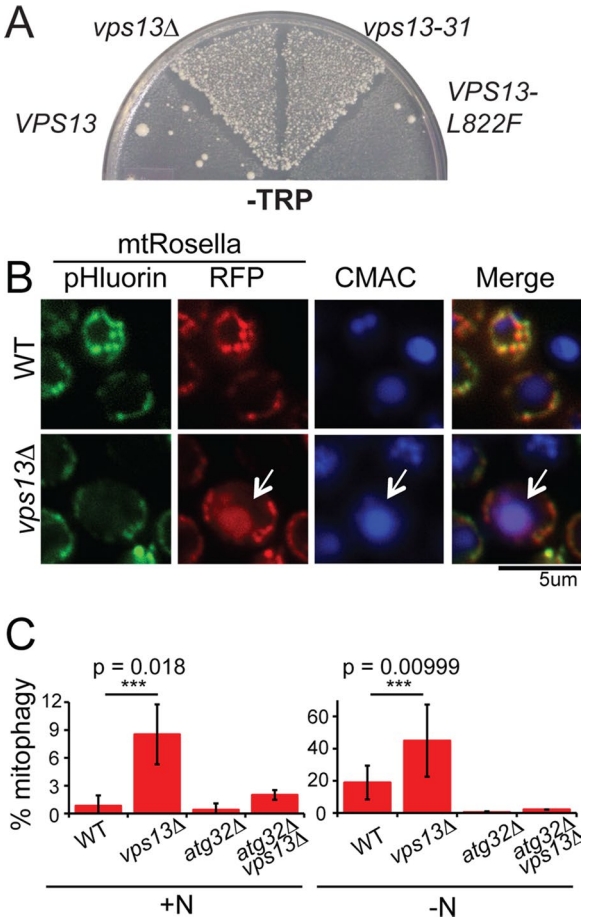

FIGURE 1: Mitochondrial phenotypes of *vps13* alleles. (A) mtDNA escape assay. Wild-type WT; PTY44), *vps13*Δ (JKY2), *vps13-31* (PTY66), and *VPS13-L822F* (MTY71) strains carrying a chromosomal *TRP1* deletion, an insertion of *TRP1* into the mitochondrial genome, and the indicated *VPS13* alleles were grown as patches on complete ethanol/glycerol medium at 30°C for 2 d and then replica plated to minimal glucose medium lacking tryptophan (–Trp) to select for transfer of *TRP1* to the nuclear DNA and incubated for 5 d at 30°C. The number of papillae growing in each sector reflects the frequency of transfer of mtDNA to the nucleus for that strain (Thorsness and Fox, 1993). (B) Mitophagy assay in WT (BY4741) and *vps13*Δ (KO1) cells grown in YPA expressing mtRosella, a fusion protein between a pH-sensitive GFP called pHluorin and RFP. Staining with the vacuolar lumen dye blue CMAC was used to determine the position of the vacuole. Scale bar, 5 μm. (C) Quantification of mitophagy assay in cells grown with or without nitrogen. The percentage of cells in the culture displaying mitophagy (indicated by red vacuolar fluorescence) was assessed in WT (BY4741), *vps13*Δ (KO1), *atg32* (KO5), and *vps13*Δ *atg32*Δ (JSP461-1) cells expressing mtRosella and grown in the presence of nitrogen (+N) or the absence of nitrogen for 5.5 h to induce mitophagy (–N). The averages from three biological replicates are plotted with error bars representing the SD. At least 200 cells were analyzed for each strain in each replicate. Asterisks indicate a statistically significant difference as assessed by Student's *t* test.

creating a frameshift that truncates the protein from 3147 to 533 amino acids (Table 1). Consistent with *vps13-31* being a null mutant, *vps13Δ* exhibited a similar high level of Trp^+ papillae.

Although *vps13* mutants show no respiration defects, that is, they are competent to grow on nonfermentable carbon sources, the mitochondrial escape phenotype suggests that mitochondria are more fragile and susceptible to breakage and DNA release

VPS13 allele	Nucleotide change	Amino acid change
VPS13	None	None
vps13-31	G 1565Δ	Codon 533 stop
VPS13-P268R	C 803 G	Pro 268 Arg
VPS13-G718K[a]	G 2152 T	Gly 718 Lys
VPS13-G718K[a]	G 2152 T	Gly 718 Lys
VPS13-G718D	G 2153 A	Gly 718 Asp
VPS13-G820R	G 2458 C	Gly 820 Arg
VPS13-G820D[b]	G 2459 A	Gly 820 Asp
VPS13-L822F[c]	G 2466 T	Leu 822 Phe
VPS13-L984S	T 2951 C	Leu 984 Ser
VPS13-V1210E	T 3629 A	Val 1210 Glu
VPS13-G1245S	G 3733 A	Gly 1245 Ser
VPS13-N1467H	A 4399 C	Asn 1467 His
VPS13-A1512E	C 4535 A	Ala 1512 Glu

[a]Mutation was recovered in two independently isolated suppressor strains.
[b]Originally designated *YNT61-1* (Hanekamp et. al., 2002).
[c]Originally designated *YNT61-3* (Hanekamp et. al., 2002).

TABLE 1: Sequence changes of *VPS13* mutant alleles.

(Campbell and Thorsness, 1998). These unstable mitochondria might therefore exhibit other phenotypes as well. Mitophagy is a specialized type of autophagy induced by nitrogen starvation in which mitochondria are degraded in the vacuole (Kanki *et al.*, 2009; Okamoto *et al.*, 2009). Mitophagy can be assayed using the marker mtRosella, which consists of a red fluorescent protein (RFP) and a pH-sensitive green fluorescent fusion protein (pHluorin) that is targeted to the mitochondrial matrix (Rosado *et al.*, 2008; Mijaljica *et al.*, 2011). In the mitochondrion, both moieties fluoresce, and overlapping green and red fluorescence is seen in the microscope. However, if the mitochondrion is degraded in the vacuole by autophagy, mtRosella is delivered to the vacuolar lumen. Vacuoles can be visualized with a blue fluorescent dye, 7-amino-4-chloromethylcoumarin (CMAC; Stefan and Blumer, 1999). Whereas mtRosella is resistant to vacuolar proteolysis, the lower pH of the vacuolar lumen specifically inhibits the green fluorescence (Mijaljica *et al.*, 2011). Therefore red fluorescent vacuoles serve as an indicator of mitophagy.

VPS13 suppresses basal levels of mitophagy, as a fivefold increase in red fluorescing vacuoles was observed in *vps13Δ* cells grown in the presence of nitrogen (Figure 1, B and C; Kanki *et al.*, 2009; Okamoto *et al.*, 2009). As previously reported, the absence of nitrogen caused an increase in the fraction of wild-type cells exhibiting mitophagy (Kanki *et al.*, 2009; Okamoto *et al.*, 2009). The frequency of mitophagy was further increased threefold in *vps13Δ* (Figure 1C). *VPS13* suppresses the canonical mitophagy pathway, as the increase in red-fluorescing vacuoles depended on *ATG32*, a gene that is specifically required for mitophagy (Figure 1C; Kanki *et al.*, 2009; Okamoto *et al.*, 2009). The requirement for *VPS13* in preventing mitochondrial escape and mitophagy indicates a new role for *VPS13* in promoting the structural integrity of mitochondria.

Dominant mutants in *VPS13* suppress *mmm1*Δ

Deletion of *MMM1* results in slow growth on glucose medium, abnormal mitochondrial morphology, and failure to grow on nonfermentable carbon sources (Hobbs *et al.*, 2001; Figure 2). Further

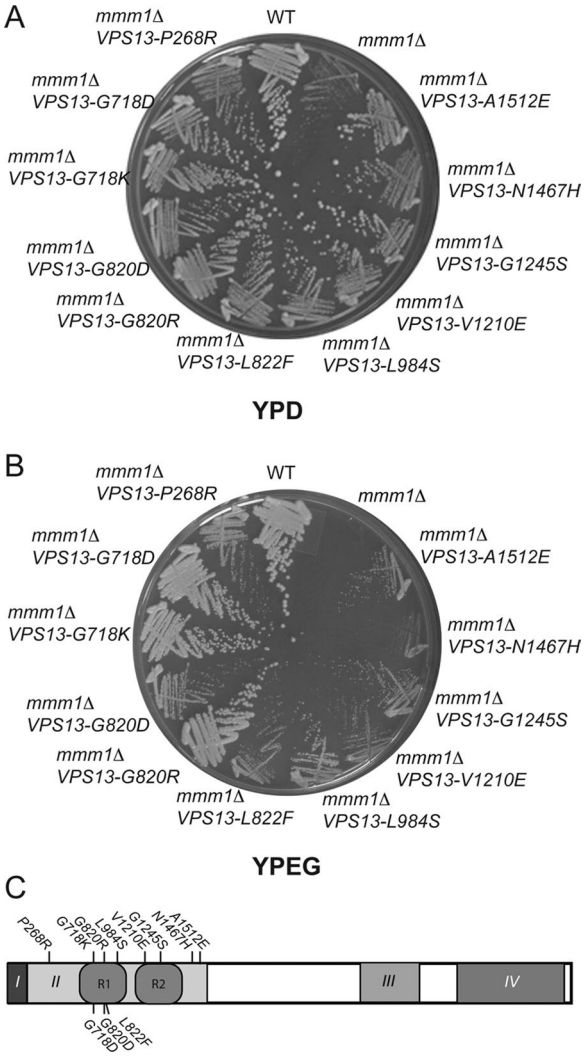

FIGURE 2: *VPS13* suppressors of *mmm1*Δ. Yeast strains containing *mmm1*Δ and various alleles of *VPS13* were streaked for single colonies on the indicated medium and incubated from 3 to 5 d at 30°C. Strains: WT, PTY44; *mmm1Δ*, THY23; *mmm1Δ VPS13-A1512E*, KWY114; *mmm1Δ VPS13-N1467H*, KWY76; *mmm1Δ VPS13-G1245S*, KWY105; *mmm1Δ VPS13-V1210E*, KWY75; *mmm1Δ VPS13-L984S*, KWY111; *mmm1Δ VPS13-L822F*, MTY79; *mmm1Δ VPS13-G820R*, KWY70; *mmm1Δ VPS13-G820D*, JHY14; *mmm1Δ VPS13-G718K*, KWY109; *mmm1Δ VPS13-G718D*, KWY131; *mmm1Δ VPS13-P268R*, KWY80. (A) Growth on 2% glucose medium (YPD). (B) Growth on 3% ethanol/3% glycerol medium (YPEG). (C) Location of *VPS13* mutations that suppress the *mmm1Δ* growth defect. Conserved domains of Vps13 are indicated by roman numerals I–IV (not drawn to scale; Velayos-Baeza *et al.*, 2004). I, N-chorein domain; II ,repeat containing domain (position of repeats shown by R1 and R2); III, DUF1162 domain; IV, C-terminal domain. Positions of the amino acid changes in the suppressor alleles are indicated (see also Table 2).

evidence of a role for *VPS13* in mitochondrial function came from the discovery that several spontaneous dominant suppressors of the *mmm1*Δ growth defect are nonnull alleles of *VPS13* (Hanekamp *et al.*, 2002; Table 1 and Figure 2A). Mutants in *MMM1* rapidly lose mtDNA (Hobbs *et al.*, 2001). Therefore, to determine whether the *VPS13* dominant suppressors bypass the requirement for *MMM1* for respiration, it was necessary to first reintroduce mtDNA into the *VPS13-X mmm1Δ* deletion strains. This was done by crossing each

strain to a ρ^+ haploid, sporulating the diploids, and dissecting tetrads to get haploid segregants. *VPS13-X mmm1Δ* ρ^+ strains were then tested for their ability to respire by looking at growth on the plates containing ethanol and glycerol as the sole carbon sources. All of the *VPS13* alleles bypassed the *MMM1* requirement for respiration, with growth rates ranging from slow to nearly wild type (Figure 2B). The mechanism by which these dominant mutants suppress *MMM1* appears to be independent of mitochondrial integrity, as these mutants exhibited a low level of mitochondrial escape equivalent to wild type (e.g., *VPS13-L822F* is shown in Figure 1A).

Vps13 family proteins have four major regions of conservation (Velayos-Baeza *et al.*, 2004; Figure 2C). The highest level of conservation is found within the first 100 amino acids (aa) in what is termed the N-chorein domain (domain I in Figure 2C). This is followed by an ~1200- aa conserved region (domain II), a DUF1162 domain of ~300 aa (domain III), and then an ~500-aa region of homology related to the Atg2 protein (domain IV; Velayos-Baeza *et al.*, 2004). All of the suppressor alleles are missense mutations that localize within domain II (Figure 2C and Table 1). In the yeast Vps13, domain II includes two copies of a repeated region with a core P-X_4-P-$X_{13\text{-}17}$-G motif (Velayos-Baeza *et al.*, 2004; shown as R1 and R2 in Figure 2C). Four of the independently isolated suppressors mutated a conserved glycine in one or the other of these repeats, and many of the remaining suppressor alleles fall within R1 or R2. Lang *et al.* (2015) recently reported the isolation of five different mutations in *VPS13* that suppress the growth defect of *mmm1Δ* or deletions of other ERMES subunits. All five of these mutations fall into domain II as well. Thus alteration of this region of the protein seems particularly prone to giving rise to *mmm1Δ* suppressors. Both *vps13Δ* and *mmm1Δ* exhibit a mitochondrial escape phenotype, the two mutants are synthetically lethal, and gain-of-function alleles of *VPS13* can bypass *mmm1Δ* for respiration. Taken together, these observations suggest that *VPS13* acts in parallel to ERMES to support mitochondrial homeostasis.

Green fluorescent protein fusions create separation-of-function alleles of *VPS13*

A C-terminal fusion of Vps13 to green fluorescent protein (GFP; *vps13-GFP$_C$*) exhibits wild-type levels of sporulation (Park and Neiman, 2012; Table 2). *VPS13* and *VPS10* (which encodes the CPY receptor in the vacuole) are both required for delivery of CPY to the vacuole (Bankaitis *et al.*, 1986). In the absence of these genes, a fraction of the CPY is missorted at the Golgi and secreted (Bankaitis *et al.*, 1986; Figure 3B). No secreted CPY was observed in the *vps13-GFP$_C$* strain, however, indicating that this allele is functional for CPY sorting (Figure 3B).

In contrast, *vps13-GFP$_C$* is synthetically lethal with *mmm1Δ*, indicating that it lacks the *VPS13* function that compensates for the lack of ERMES (Figure 3, C and D; Lang *et al.*, 2015). This was demonstrated in two ways. First, a *VPS13/vps13-GFP$_C$ mmm1Δ::kanMX6/MMM1* double heterozygote was sporulated and the tetrads dissected. Given that *VPS13* and *MMM1* are unlinked, one-fourth of the spores should be double mutants. However, no viable *vps13-GFP$_C$ mmm1Δ*::kanMX6 segregants were obtained from the dissection of 18 tetrads (Figure 3C; p <0.001, χ^2 test). Second, *vps13Δ mmm1Δ* strains are viable when they contain a replicating plasmid carrying *MMM1* and *URA3* as a selectable marker (Figure 3D). Because loss of the *MMM1* gene on the plasmid is lethal, *vps13Δ mmm1Δ*/pRS316-*MMM1* cells cannot grow on medium containing the drug 5-fluoroorotic acid (5-FOA), which kills cells containing *URA3* (Boeke *et al.*, 1987). Similarly, a *vps13-GFP$_C$ mmm1Δ*/pRS316-*MMM1* strain did not grow on 5-FOA (Figure 3D). In contrast, the

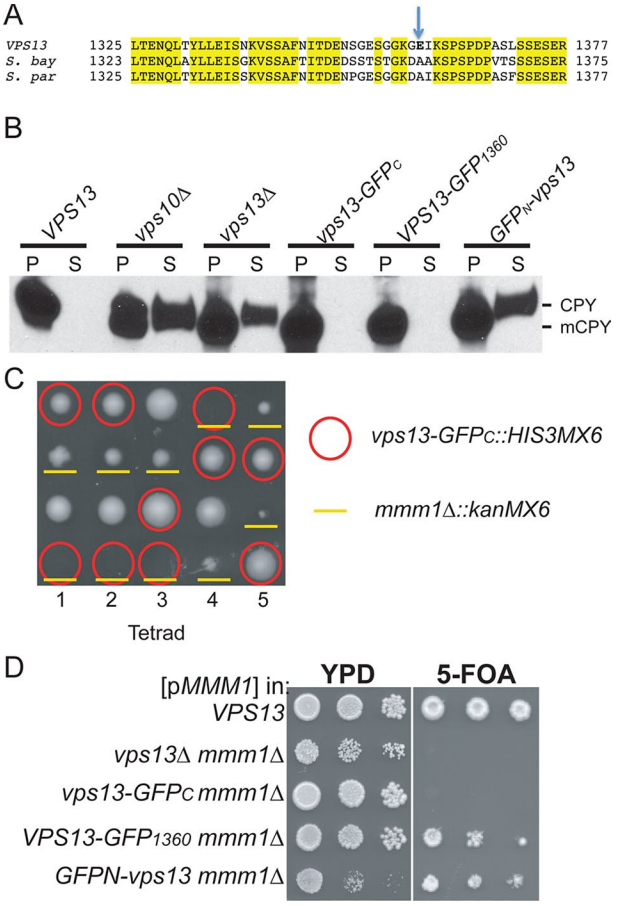

FIGURE 3: Phenotypes of different GFP-tagged *VPS13* alleles. (A) Insertion site for the *VPS13-GFP$_{1360}$* allele. Alignment of the predicted sequence of a region of *S. cerevisiae VPS13* with those from the closely related yeasts *Saccharomyces bayanus* and *Saccharomyces paradoxus*. GFP was integrated as an in-frame insertion immediately after the residue indicated by the arrow. (B) CPY sorting. Overnight cultures of WT (BY4741), *vps10Δ* (KO3), *vps13Δ* (KO1), *vps13-GFP$_C$* (GCY1), *VPS13-GFP$_{1360}$* (JSP497), and *GFP$_N$-vps13* (JSP513) strains were separated by centrifugation into pellet (P) and supernatant (S) fractions. The proteins in the supernatant were precipitated with TCA, and the P and S samples were probed on a Western blot with anti-CPY antibodies. mCPY indicates the processed, vacuolar form of the protein. (C) Synthetic lethality of *vps13-GFP$_C$* with *mmm1Δ* shown by tetrad analysis. An *MMM1/mmm1Δ::kanMX6 VPS13/vps13-GFP$_{C::}$HIS3MX6 his3/his3* diploid, JSYD10, was sporulated and five tetrads dissected onto a YPD plate. Spores containing *vps13-GFP$_{C::}$HIS3MX6* are indicated by red circles, and *mmm1Δ::kanMX6* is indicated by yellow underlines. (D) Synthetic lethality of different *VPS13 GFP* fusions with *mmm1Δ* shown by plasmid loss. Haploid WT (BY4741), *vps13Δ mmm1Δ* (JSP443), *vps13-GFP$_C$ mmm1Δ* (JSP577), *VPS13-GFP$_{1360}$ mmm1Δ* (LUKE3), or *GFP$_N$-vps13 mmm1Δ* (JSP491) carrying pRS316-*MMM1* strains were grown overnight at 30°C in YPD. Tenfold serial dilutions were spotted onto YPD or SD complete medium containing 5-FOA and grown at 30°C for 3 d.

MMM1 gene could be lost from the *VPS13* control. Therefore fusion of *GFP* to the end of *VPS13* creates an allele that is specifically defective in the ability of *VPS13* to compensate for the loss of ERMES.

To create a fully functional *GFP*-tagged version of *VPS13* for protein localization studies, *GFP* was either fused at the 5′ end of the gene (*GFP$_N$-vps13*) or inserted in-frame between codons 1359 and 1360 of the gene (*VPS13-GFP$_{1360}$*). This region of *VPS13* was

Strain[a]	Relevant genotype	Percentage sporulation[b]
JSYD1	*VPS13/VPS13*	53 ± 8
JSYD2	*vps13Δ/vps13Δ*	0 ± 0
JSYD3	*vps13Δ/vps13-GFP$_C$*	53 ± 4
JSYD4	*vps13Δ/VPS13-GFP$_{1360}$*	59 ± 1
JSYD5	*vps13Δ/GFP$_N$-vps13*	1 ± 1
JSYD6	*vps13Δ/vps13-L66P*	64 ± 1
JSYD7	*vps13Δ/vps13-C89K*	55 ± 3
JSYD8	*vps13Δ/vps13-L1107P*	40 ± 3
JSYD9	*vps13Δ/vps13-Y2702C*	48 ± 5

[a]Hybrid diploids were created by mating haploids from the BY4741 background to the SK1 *vps13Δ* strain, HI27.

[b]Averages from at least three colonies are shown with the SD. At least 200 cells were scored for each colony.

TABLE 2: Sporulation efficiency of different *VPS13* alleles.

chosen because it encodes a patch of lower amino acid conservation, as determined by alignment of the *S. cerevisiae VPS13* with orthologues from closely related yeasts (Figure 3A). The *GFP$_N$-vps13* allele displayed phenotypes complementary to that of *vps13-GFP$_C$*: the *GFP$_N$-vps13* diploid did not sporulate (Table 2), CPY was secreted, similar to *vps10Δ* and *vps13Δ* (Figure 3B), and *GFP$_N$-vps13* was viable when combined with *mmm1Δ* (Figure 3D). By contrast, cells expressing *VPS13-GFP$_{1360}$*, appeared wild type in all three assays (Figure 3 and Table 2). These results demonstrate that three different processes known to require *VPS13*—sporulation, vacuolar sorting, and viability in the absence of *MMM1*—are genetically separable, suggesting that they result from loss of different aspects of *VPS13* function. Moreover, *VPS13-GFP$_{1360}$* seems to be fully functional, making it a useful reagent for localization studies.

Vps13 localizes to membrane contact sites

Like Vps13-GFP$_C$, Vps13-GFP$_{1360}$ localized to the prospore membrane in sporulating cells (Huh *et al.*, 2003; Park and Neiman, 2012; Figure 4A). Consistent with studies using Vps13-GFP$_C$ in vegetative cells, Vps13-GFP$_{1360}$ was present in foci of which ~85% colocalized with the late endosomal marker Did2–monomeric RFP (mRFP), suggesting that Vps13 localizes primarily to the endosome (Figure 4B; Huh *et al.*, 2003; Lottridge *et al.*, 2006).

Vps13-GFP$_{1360}$ localization in a strain containing the mitochondrial marker mitochondrial blue fluorescent protein (mtBFP; Westermann and Neupert, 2000) revealed that ~20% of the Vps13 puncta colocalized with mitochondria. When markers for Vps13, mitochondria, and endosomes were all present in the same cell, 91% of the Vps13GFP$_{1360}$ foci that overlapped with mtBFP also overlapped with Did2-mRFP (Figure 4C). That is, a fraction of the Vps13 in the cells is localized at sites where endosomal and mitochondrial membranes are in close proximity.

The localization of the three markers at these sites characteristically shows overlap between the Vps13 signal and the mitochondrial signal and overlap between the endosomal signal and Vps13 but little or no overlap between the endosome and the mitochondrion (Figure 4C). That is, Vps13 sits at the interface between the endosome and mitochondrion, suggesting that it is a component of a contact site between the endosomal and mitochondrial membranes. To our knowledge, this is the first identification of a protein at endosome–mitochondrial contacts.

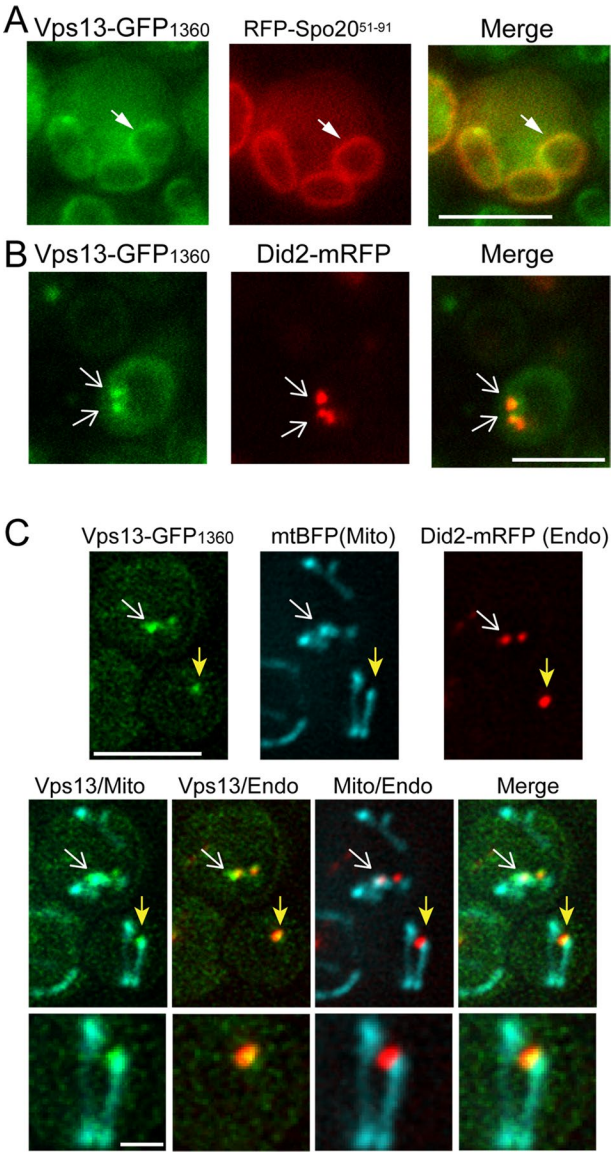

FIGURE 4: Localization of Vps13-GFP$_{1360}$ in vegetative and sporulating cells. (A) Prospore membrane localization. The SK1 diploid JSP528 carrying pRS426-R20 was transferred to Spo medium for 6–8 h. The pRS426-R20 plasmid contains a protein fragment from Spo20 fused to RFP (RFP-Spo20$^{51–91}$) that localizes to prospore membranes (Suda *et al.*, 2007). White arrowheads indicate one prospore membrane of a developing tetrad. (B) Endosome localization. A strain expressing both *VPS13-GFP$_{1360}$* and a tagged version of the late endosome marker *DID2-mRFP* (JSP527) was grown to mid log phase in synthetic glucose medium and analyzed by fluorescence microscopy. White arrows indicate overlapping foci. Of 655 total Vps13-GFP$_{1360}$ foci examined over four experiments, 561 displayed colocalization with Did2-mRFP. (C) Endosome and mitochondrial localization. Cells expressing Vps13-GFP$_{1360}$, Did2-mRFP (Endo), and mtBFP (Mito; JSP512/pVT100U-mtBFP) were analyzed as in B. Arrows indicate sites where Vps13-GFP$_{1360}$ colocalizes with both the endosomal and mitochondrial markers. Of 423 total Vps13-GFP$_{1360}$ foci examined in two experiments, 97displayed colocalization with mtBFP. Of these 97, 87 also colocalized with Did2-mRFP. Scale bar, 5 μm. Bottom, higher magnification of the focus indicated by the yellow arrow. Scale bar, 1 μm.

Vps13 moves to the prospore membrane in sporulation medium, in which acetate is the carbon source (Park and Neiman, 2012). *VPS13* is important for mitochondrial homeostasis (Figure 1), and

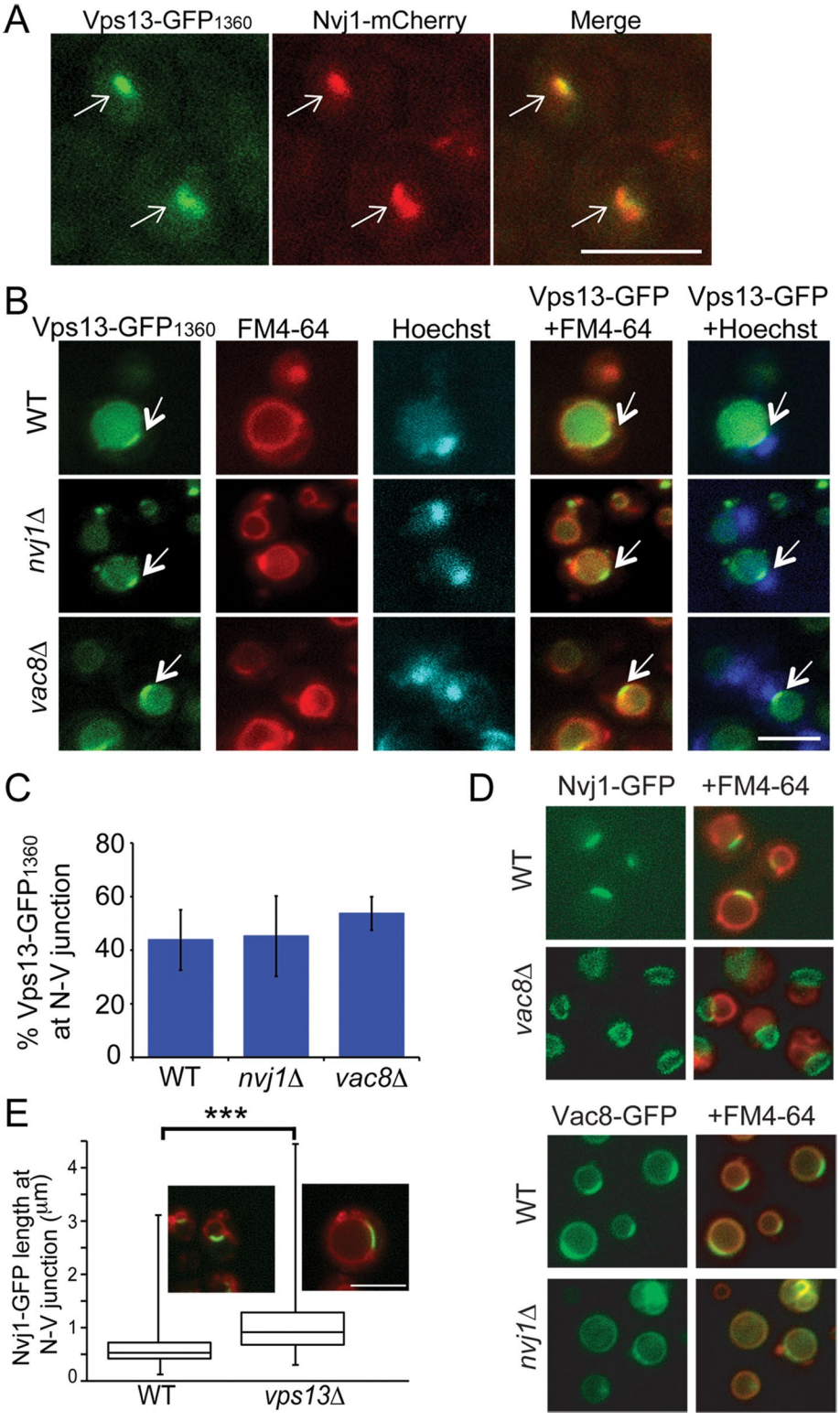

FIGURE 5: Vps13 localization in acetate medium. (A) Vps13-GFP$_{1360}$ localization in cells (JSP552) growing in YPA medium. The NV junction was marked using Nvj1-3xmCherry. White arrows point to foci containing both Vps13-GFP$_{1360}$ and Nvj1-3xmCherry. (B) Vps13-GFP$_{1360}$ localization in NV junction mutants. *VPS13-GFP$_{1360}$* (JSP497), *VPS13-GFP$_{1360}$ nvj1*Δ (JSP541), and *VPS13-GFP$_{1360}$ vac8*Δ (JSP545) cells were grown in YPA and stained with FM4-64 and Hoechst to mark the vacuolar membranes and nuclei, respectively. White arrows indicate GFP fluorescence at the NV junction. (C) Quantification of the localization pattern shown in B. Percentages are the averages of four experiments (at least 100 cells scored in each experiment). Error bars indicate the SD. (D) *NVJ1* and *VAC8* are codependent for localization to the NV junction. Nvj1-GFP localization was examined in WT (GCY3) and *vac8*Δ (JSP555) cells, and Vac8-GFP was examined in WT (GCY4) and *nvj1*Δ (JSP547). Cells were labeled with FM4-64 to visualize the vacuolar membrane. (E) The length of NV junctions as marked by Nvj1-GFP fluorescence was measured in *VPS13* (GCY3) and *vps13*Δ (JSP536) cells grown in YPA. Insets, merged images of green (Nvj1-GFP) and red (FM4-64) fluorescence for a representative cell from each culture. The average length of the GFP fluorescence at the NV junction was plotted. The horizontal line indicates the median value, the boxes represent three quartiles, and the whiskers denote the range of values. More than 790 cells in each strain were measured. Asterisks indicate a significant difference ($p < 0.0001$ as calculated by Student's *t* test). Scale bars, 5 μm.

growth on nonfermentable carbon sources such as acetate requires mitochondria. Localization of Vps13-GFP$_{1360}$ was therefore examined in cells grown in yeast extract/peptone/acetate (YPA) medium (Figure 5). When acetate was the sole carbon source, the localization of Vps13-GFP$_{1360}$ was altered, with many cells displaying green fluorescence along one edge of the vacuole (Figure 5, A and B). This pattern is reminiscent of nuclear–vacuolar (NV) junctions, which are formed where the vacuole contacts the nuclear envelope (Pan *et al.*, 2000). NV junctions are created by the interaction of the integral ER protein Nvj1 with the peripheral vacuolar membrane protein Vac8 (Pan *et al.*, 2000). Vps13-GFP$_{1360}$ colocalized with an Nvj1-3xmCherry marker protein in cells grown in YPA, demonstrating that Vps13 is present at NV junctions (Figure 5A), as was also observed by Lang *et al.* (2015). Thus the localization of Vps13 at different membrane contact sites varies, depending upon the carbon source.

Interaction of Nvj1 with Vac8 is necessary to recruit other proteins to the NV junction (Kvam and Goldfarb, 2004; Kvam *et al.*, 2005). To determine whether *NVJ1* or *VAC8* is necessary to recruit Vps13, we examined the localization of Vps13-GFP$_{1360}$ in *nvj1Δ* and *vac8Δ* cells. Cells were stained with both FM4-64 and Hoechst to visualize the vacuolar membrane and nucleus, respectively. The position of the NV junction is defined as the site where the nucleus abuts the vacuolar membrane (Pan *et al.*, 2000). Vps13-GFP$_{1360}$ was concentrated at the interface of the vacuole and nucleus to comparable degrees in wild-type, *nvj1Δ*, and *vac8Δ* strains (Figure 5. B and C). This result is in contrast to a recent report that Vps13 localization to the NV junction depends on *NVJ1* (Lang *et al.*, 2015). This discrepancy is not due to a problem with the assay, as delocalization of Nvj1 and Vac8 was observed

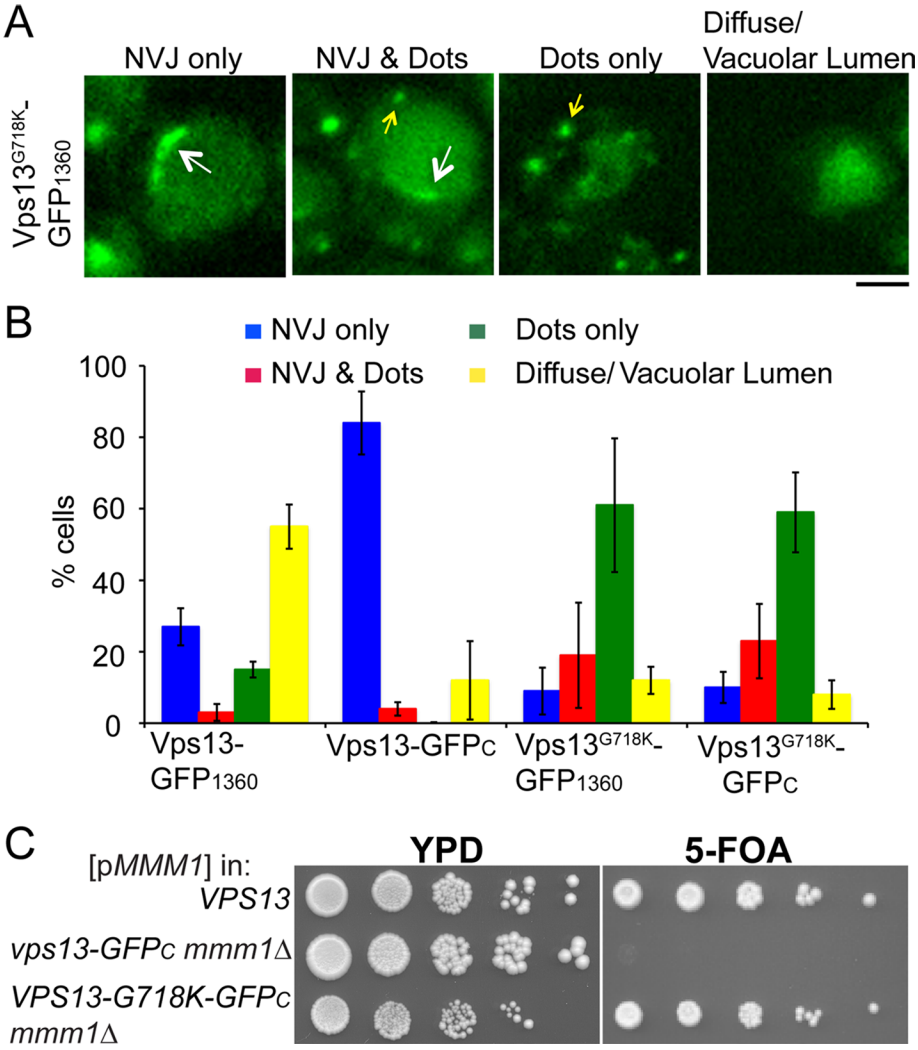

FIGURE 6: The effect of the GFP_C tag and the G718K mutation on Vps13 localization. Cells expressing *VPS13-GFP*$_{1360}$ (JSP497) or *vps13-GFP*$_C$ (GCY1), *VPS13-G718K-GFP*$_{1360}$ (JSP531), or *VPS13-G718K -GFP*$_C$ (JSP556) were grown in YPA, and the pattern of Vps13-GFP distribution in individual cells was categorized. (A) Representative cells for each pattern. Scale bar, 5 μm. (B) The distribution of cells in each category in the four different strains. Average percentages from three experiments (at least 200 cells scored in each). Error bars indicate the SD. (C) Suppression of the *vps13-GFP*$_C$ *mmm1Δ* synthetic lethal phenotype by the G718K mutation. Serial dilutions of WT (BY4741), *vps13-GFP*$_C$ *mmm1Δ* (JSP577), and *vps13-G718K-GFP*$_C$ *mmm1Δ* (JSP590) carrying pRS316-*MMM1* were spotted on YPD or SD complete medium with 5-FOA.

The intracellular distribution of Vps13 correlates with function

The *vps13-GFP*$_C$ mutant is synthetically lethal with *mmm1Δ*, and, conversely, dominant mutations such as *VPS13-G718K* suppress the *mmm1Δ* growth phenotype. To determine whether changes in Vps13 localization are correlated with these differences in activity, we examined the localization of Vps13-GFP_C, Vps13-GFP_{1360}, and $Vps13^{G718K}$-GFP_{1360} in YPA-grown cells. The localization patterns within individual cells were classified into four different categories: NV junctions only; NV junctions and cytoplasmic foci ("dots"); cytoplasmic foci only; and cells in which the signal was diffuse in the cytosol or only in the vacuolar lumen (the latter suggesting degradation of the fusion protein; Figure 6A). The Vps13-GFP_C protein localized more extensively than Vps13-GFP_{1360} to NV junctions and was not present in cytoplasmic dots, suggesting that the absence of "dots" may be responsible for the synthetic lethal phenotype observed between *vps13-GFP*$_C$ and *mmm1Δ*. In contrast, the number of cells with only dots was increased by introduction of the G718K mutation compared with Vps13-GFP_{1360} (Figure 6B). The localization of Vps13-GFP_C containing G718K was similarly shifted away from NV junctions to cells with dots. Furthermore, the introduction of the G718K mutation into *vps13-GFP*$_C$ suppressed the synthetic lethality with *mmm1Δ* (Figure 6C). Lang *et al.* (2015) observed a similar result using a different *VPS13* mutant. We conclude that the Vps13-GFP_C protein fails to reach some location at which its activity is critical to compensate for the loss of ERMES and that mutations in the region around G718 redistribute Vps13 back to this location.

Human disease–associated *VPS13A* mutations introduced into yeast *VPS13* are synthetically lethal with *mmm1Δ*

To elucidate why mutations in *VPS13A* in humans cause a neurodegenerative disorder, it would be helpful to determine which *VPS13*-dependent processes are affected by these mutations. Most of the identified *VPS13A* mutations are deletions or splice junction mutations that likely generate null alleles; however, six missense alleles have been identified in patient samples (Rampoldi *et al.*, 2001; Dobson-Stone *et al.*, 2002; Tomiyasu *et al.*, 2011). Alignment of Vps13A with yeast Vps13 identified cognate residues in the yeast protein for four of the amino acids changed by the missense mutations (Figure 7A). We then characterized *VPS13* alleles in which these cognate amino acids were individually substituted with the amino acids encoded in the *VPS13A* disease alleles (L66P, C89K, L1107P, Y2702C; Figure 7B) for effects on sporulation, vacuolar sorting, and synthetic lethality with *mmm1Δ*.

No obvious phenotypes were observed for *VPS13-Y2702C*, indicating that this mutation does not alter the function of the yeast

in *vac8Δ* and *nvj1Δ* strains, respectively (Figure 5D; Pan *et al.*, 2000). Our data indicate that Vps13 is recruited to the nuclear envelope–vacuole interface independently of the canonical NV junction architectural proteins.

Different membrane contact sites can respond to one another (Elbaz-Alon *et al.*, 2014, 2015; Honscher *et al.*, 2014). That is, loss of one membrane contact site produces compensatory expansion of other sites. When wild-type and *vps13Δ* cells grown in YPA were compared, the region of Nvj1 localization was more extensive in the *vps13Δ* mutant (Figure 5E). Measurement of the length of the Nvj1-GFP fluorescence along the nuclear envelope–vacuole interface in wild type and *vps13Δ* confirmed that Nvj1-containing junctions were longer in the *vps13Δ* cells (Figure 5E). Thus loss of *VPS13* can lead to expansion of Nvj1-containing NV junctions, perhaps to compensate for the loss of Vps13-containing junctions.

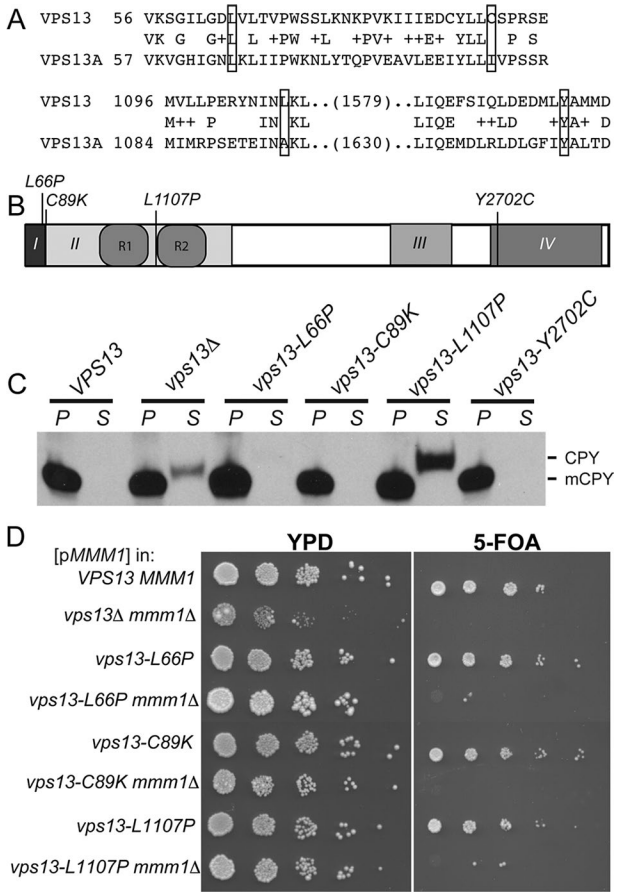

FIGURE 7: Phenotypes of human *VPS13A* ChAc mutations introduced into yeast *VPS13*. (A) Alignment of the Vps13 amino acid sequence with Vps13A. Residues that were mutated are boxed. The cognate amino acid substitutions encoded by the mutations are as follows: Vps13A L67P = Vps13 L66P; Vps13A I90K = Vps13 C89K; Vps13A A1095P = Vps13 L1107P; and Vps13A Y2721C = Vps13 Y2702C. (B) Vps13 domain structure showing the position of the disease alleles in yeast Vps13. Amino acid changes listed above are the position of the yeast *VPS13* residues. (C) CPY sorting in the *vps13* mutants containing the cognate *vps13A* disease mutations performed as in Figure 3A. Strains assayed: WT (BY4741) *vps13Δ* (KO1), *vps13-L66P* (RP201), *vps13-C89K* (RP205), *vps13-L1107P* (RP202), and *vps13-Y2702C* (RP203). mCPY indicates the mobility of the processed, vacuolar form of the protein. (D) Assay for synthetic lethality between *vps13* mutants containing the cognate *vps13A* disease mutations and *mmm1Δ*, assayed as in Figure 3C. Strains: WT (BY4741), *vps13Δ mmm1Δ* (JSP446), *vps13-L66P* (RP201), *vps13-L66P mmm1Δ* (RP301), *vps13-C89K* (RP205), *vps13-C89K mmm1Δ* (JSP582), *vps13-L1107P* (RP202), and *vps13-L1107P mmm1Δ* (JSP585).

protein for these processes. All of the mutants were proficient for sporulation (Table 2). The *vps13-L1107P* strain showed a defect in CPY sorting, whereas *vps13-L66P* and *C89K* behaved like wild type (Figure 7C). The phenotype in common for *vps13-L66P*, *vps13-C89K*, and *vps13-L1107P* was synthetic lethality with *mmm1Δ* (Figure 7D). Thus the inability to compensate for the loss of ERMES is associated with missense mutants that cause disease in humans.

The *G718K* mutation rescues the synthetic lethality of *vps13-L66P* and *mmm1Δ*

The *vps13-L66P* mutant is phenotypically similar to *vps13-GFP$_C$* in being specifically synthetically lethal with *mmm1Δ*. Like *vps13-GFP$_C$*, Vps13-L66P localizes primarily to NV junctions (Figure 8, A and B). The synthetic lethal interaction between *vps13-GFP$_C$* and *mmm1Δ* can be suppressed by the relocalization of Vps13-GFP$_C$ to NV junctions by the G718K mutation (Figure 6). The addition of G718K to *vps13-L66P* also redistributed the protein within the cells and suppressed the synthetic lethal phenotype with *mmm1Δ* (Figure 8, B and C). Thus the distribution of Vps13 within the cell correlates with its ability to promote mitochondrial homeostasis.

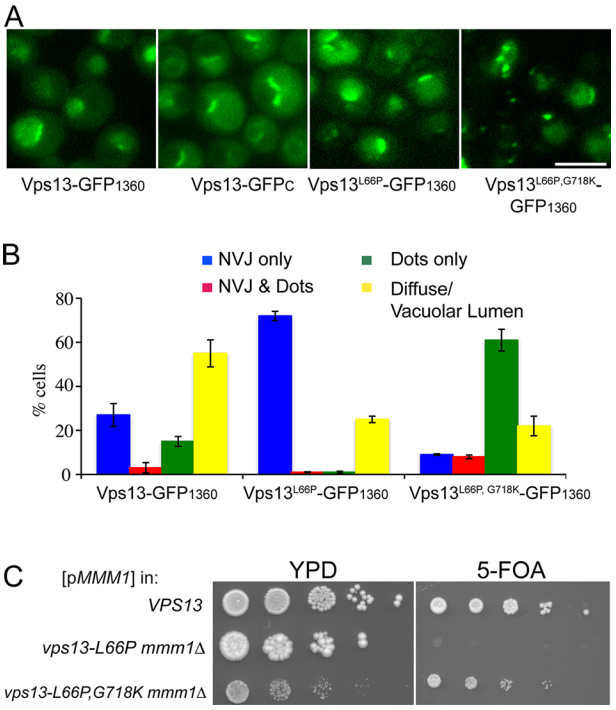

FIGURE 8: Effect of the G718K mutation on *vps13-L66P* phenotypes (A) Representative images of cells expressing *VPS13-GFP$_{1360}$* (JSP497), *vps13*-GFP$_C$ (GCY1), *vps13-L66P-GFP$_{1360}$* (JSP560), or *vps13-L66P, G718K-GFP$_{1360}$* (JSP563) grown in YPA medium. Scale bar, 5 μm. (B) Quantification of the localization patterns for proteins in A. Data for Vps13-GFP$_{1360}$ are from Figure 6B. Average percentages from three experiments (at least 200 cells scored in each). The error bars indicate the SD. (C) Synthetic lethality with *mmm1Δ*. Tenfold serial dilutions of WT (BY4741), *vps13-L66P mmm1Δ* (RP301), and *vps13-L66P,G718K mmm1Δ* (JSP533) cells carrying pRS316-*MMM1* were spotted onto either YPD or SD complete with 5-FOA.

DISCUSSION

VPS13 is important for mitochondrial integrity

The synthetic lethality between null alleles of *VPS13* and components of the ERMES complex suggests that *VPS13* is somehow involved in mitochondrial function, but this connection could be indirect. This work demonstrates that *VPS13* promotes mitochondrial integrity even when ERMES function is intact. *VPS13* is required to prevent mitochondrial DNA from being transferred to the nucleus, an indicator of mitochondrial stability. Furthermore, *VPS13* is required to prevent autophagy of mitochondria by the vacuole, a phenomenon that may be stimulated by less stable mitochondria. Whether the contribution of *VPS13* to mitochondrial integrity is structural or is the result of a more indirect effect, for example, on lipid levels as is observed in sporulating cells, remains to be determined. What is clear is that *VPS13* is required for normal mitochondrial function.

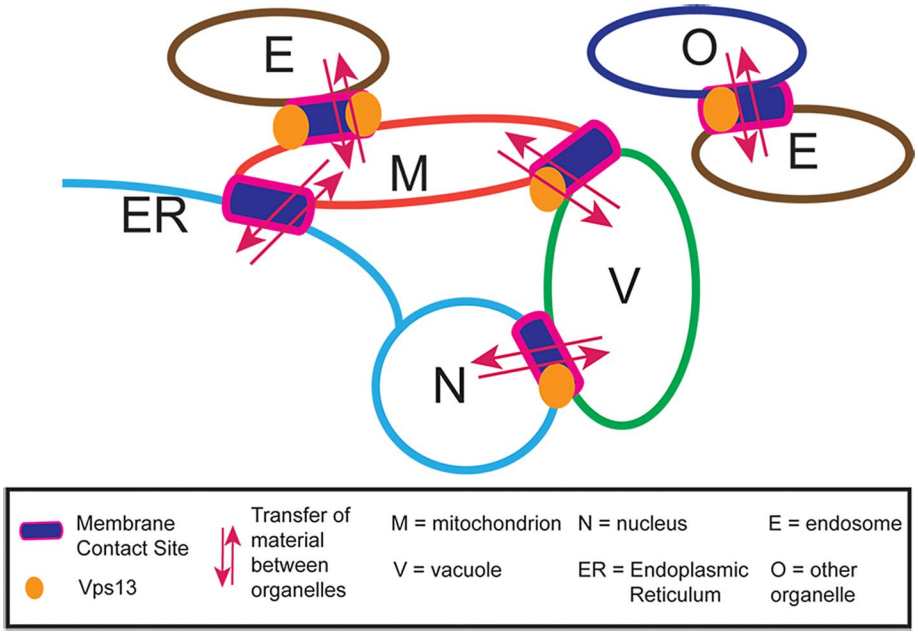

FIGURE 9: Model for Vps13 intracellular distribution. In vegetative cells, Vps13 (orange circles) is found at membrane contact sites between different organelles (purple rectangles). At these sites, Vps13 acts to enhance exchange of materials, likely phospholipids, between the organellar membranes.

Vps13 acts at membrane contact sites

There are several different types of membrane contact sites in a cell that allow communication between different organelles. Synthetic lethal interactions between components in different membrane contact sites indicate that these junctions are sometimes able to compensate for each other. For example, vCLAMP mutants are synthetically lethal with ERMES mutants (Elbaz-Alon *et al.*, 2014; Honscher *et al.*, 2014). Lang *et al.* (2015) found that Vps13 localizes to vacuole–mitochondria contact sites, perhaps as a component of vCLAMP, which may explain the requirement of *VPS13* for viability in the absence of ERMES. Our identification of Vps13 at endosome–mitochondrion contacts indicates a second possible site through which *VPS13* may act in parallel to ERMES.

Vps13 localizes to three different membrane contact sites—the NV junctions, endosome–mitochondria junctions, and vacuole-mitochondria junctions—and perhaps additional contact sites between endosomes and other organelles (Figure 9). We propose that in wild-type cells, these different membrane contact sites compete to recruit Vps13. When *VPS13* is deleted, the protein is lost from all of the contact sites, leading to pleiotropic phenotypes. Because some of the Vps13-containing contact sites act in parallel to ERMES, *vps13*Δ cells depend on ERMES for survival. Mutations or conditions that change *VPS13* distribution can phenocopy aspects of the deletion phenotype. For example, redistribution of the protein toward NV junctions depletes it from endosome–mitochondria junctions and renders the cell dependent on ERMES for growth. Conversely, redistribution of Vps13 so that it is enriched at mitochondrial contacts might increase the flow of materials into mitochondria through these routes, thereby making ERMES dispensable.

Contact sites between different combinations of organelles have been identified in both yeast and mammalian cells (Toulmay and Prinz, 2011; Schrader *et al.*, 2015). Although functions of these different membrane junctions are conserved in different organisms, many of the protein constituents are not. For example, no orthologues of either the ERMES complex or the NV junction complex protein Nvj1 have been found in metazoans. These lineage-specific complexes may therefore be more recent evolutionary innovations. In contrast, the *VPS13* family is strongly conserved, suggesting a fundamental function in eukaryotic cells. The relatively modest phenotypes of *vps13Δ* in mitotically dividing cells is consistent with the idea that Vps13-mediated junctions are redundant with other membrane contact sites. In this view, Vps13-mediated junctions are important as "back-up" systems but are only primarily responsible for mediating interorganelle traffic at a few locations and conditions such as sporulation. Contact sites generally consist of both structural proteins that act to hold the two organelles together and transfer proteins such as oxysterol-binding protein or Lam-family enzymes (Murley *et al.*, 2015; Olkkonen, 2015). Very large size (>300 kDa) is a conserved feature of Vps13 family proteins. It is possible that the protein is large enough to provide both the tethering function and lipid transfer activity, thereby creating a functional membrane contact site on its own.

Whether *VPS13* functions solely at membrane contact sites is not clear. With respect to sporulation, *VPS13* is required for wild-type levels of the lipids PtdIns-4-phosphate and PtdIns-4,5-bisphosphate in the prospore membrane (Park and Neiman, 2012). One possibility is that *VPS13* directly regulates the kinases and/or phosphatases that generate these different types of lipids. An alternative explanation is that Vps13-mediated contact sites are necessary to generate wild-type levels of PtdIns in the prospore membrane and, indirectly, PtdIns phosphate levels as well.

Regulation of Vps13 distribution

The presence of Vps13 at multiple locations raises the question of how the distribution of Vps13 is controlled. Vps13 localization varies both with growth medium and developmental stage. For sporulating cells, relocalization of Vps13 to prospore membranes requires the sporulation-specific gene *SPO71* (Park *et al.*, 2013). On induction, Spo71 binds to Vps13 and recruits it to the prospore membrane. Ectopic expression of *SPO71* changes Vps13 localization in vegetative cells (Park *et al.*, 2013). It may also be the case that different Vps13-binding proteins in vegetative cells recruit Vps13 to different sites of action. By extension, alleles that alter the function *VPS13* may result from changes in interactions with specific binding proteins. Separation-of-function alleles of Vps13 may result from a failure to interact with specific binding proteins. For example, it is striking that all the *mmm1*Δ suppressor mutations in *VPS13* have been found in domain II of the protein. One possibility is that these alleles have increased interactions with proteins at the mitochondrial–endosome interface. However, it seems unlikely that so many different mutations could increase affinity. A related possibility is that Vps13 is recruited to the NV junction through interactions between some protein and domain II. Mutations that alter the structure of domain II might reduce recruitment to the NV junction (or other some other site), making more Vps13 protein available for function at mitochondrial junctions. Similarly, alleles specifically defective in the mitochondrial homeostasis

aspect of Vps13 function, such as *vps13-L66P* and *vps13-GFP$_C$*, might interfere with binding to proteins that recruit Vps13 to the mitochondrion–endosome interface.

An alternative possibility is that the different point mutants affect levels of the protein rather than interactions with specific targeting proteins. For instance, the L66P mutation might simply lower the amount of protein, and mitochondrial homeostasis may be the activity most sensitive to Vps13 levels. Conversely, G718K might stabilize the protein, making more available to promote mitochondrial integrity. We have not been able to directly compare the levels of the proteins. However, if differences in protein stability were the basis for different phenotypes, it would still be consistent with the model that different subcellular locations compete for a limiting pool of Vps13.

The canonical NV junction is created by interaction of Nvj1 with Vac8. This interaction tethers the membranes, and, in addition, Nvj1 serves to recruit other proteins of the junction that are directly involved in material transport (Kvam and Goldfarb, 2004; Kvam *et al.*, 2005). However, contrary to a previous report (Lang *et al.*, 2015), Vps13 localization to the nuclear–vacuole interface is independent of *NVJ1* and *VAC8*, and Nvj1 junctions appear to expand in the absence of *VPS13*. Taken together, these observations suggest that Vps13 is part of an alternative NV junction complex that perhaps has overlapping functions with the Nvj1-based junctions.

VPS13 and human disease

The finding that three different *VPS13A* disease-associated mutations are specifically defective in mitochondrial homeostasis has significant implications for *VPS13*-related human diseases. This correlation suggests that the ChAc disorder arises due to a specific defect in the mitochondrial function of *VPS13A*. Tagging of the C-terminus of *VPS13* with GFP also specifically interferes with the mitochondrial homeostasis function, suggesting that the end of the protein is important for this activity. This idea is supported by the finding of a *VPS13A* mutation from ChAc patients that truncates the last 30 aa of the protein (Tomiyasu *et al.*, 2011).

This interpretation rests on the inference that the mitochondrial homeostasis function of *VPS13* is conserved in *VPS13A*. Although the localization of Vps13A has been reported in different cell types, none of these studies observed Vps13A on mitochondria (Kurano *et al.*, 2007; Hayashi *et al.*, 2012). However, localization may depend on the cell type or growth conditions. Given that ChAc is a neurodegenerative disease, it will be important to examine the possible association of Vps13A with mitochondria in mature neurons.

If mitochondrial dysfunction is the basis for the symptoms of ChAc, this would make ChAc similar to several other neurodegenerative disorders, such as Parkinson's disease, in which mitochondrial dysfunction is a common basis (Burte *et al.*, 2015). Moreover, defects in mitochondrial membrane contact sites have been suggested to be a common pathology in a variety of neurodegenerative disorders (Krols *et al.*, 2016). Thus an underlying mitochondrial defect would be consistent with this aspect of ChAc.

MATERIALS AND METHODS

Yeast strains and media

Yeast strains used for this study are listed in Table 3. Unless otherwise mentioned, standard yeast media and genetic techniques were used (Rose and Fink, 1990). Strains carrying different GFP fusions and *VPS13* point mutations were generated using a two-step clustered regularly interspaced short palindromic repeats (CRISPR)/Cas9 technique. For example, to create strain JSP497 carrying *VPS13-GFP$_{1360}$*, the *Saccharomyces kluyveri HIS3* gene was first amplified from pFA6a-HIS3MX6 (Longtine *et al.*, 1998) with primers that incorporate flanking sequences that can direct integration of the *HIS3* cassette between nucleotides 4079 and 4080 of the *VPS13* coding region. The amplified fragment was transformed into strain BY4741, and His$^+$ transformants were screened by PCR to identify strains carrying the insertion (*VPS13::HIS3MX6int1360*). The coding region for *GFP* was then amplified with primers that create an in-frame insertion of the *GFP* sequence between codons 1359 and 1360 of *VPS13*. The *VPS13::HIS3MX6int1360* strain was cotransformed with this amplified GFP and pRS425-Cas9-*Sk*HIS3-381, a *LEU2*-marked plasmid expressing both Cas9, and a guide RNA targeting the *S. kluyveri HIS3* sequence (Jin *et al.*, 2015). Leu$^+$ transformants were screened for auxotrophy for histidine, and in-frame insertion of the GFP sequence was confirmed by PCR and DNA sequencing. Insertion of GFP at the same position in *VPS13* was used to create strains JSP499-1, JSP560, and LUKE3 and was accomplished as described for JSP497, except that the starting strains were BY4742, RP201, and KO4 respectively. Similarly, *VPS13-GFP$_{1360}$* was introduced into the SK1 strains AN117-4B and AN117-16D as described, and then these strains were mated to generate the diploid JSP528. The N-terminal *GFP$_N$-VPS13* fusion in strains JSP490 and JSP513 was also created using CRISPR/Cas9, but in these cases, the *HIS3MX6* cassette and then GFP were targeted immediately upstream of the start codon. The starting strains were AN117-16D and BY4742, respectively. Strain JSP495 carrying *DID2::mRFP* was created by transforming strain GCY2 with pRS425-Cas9-*Sk*HIS3-381 to introduce a double-strand break into the *HIS3MX6* cassette 3′ of the GFP sequence as well as a PCR fragment carrying the mRFP coding region flanked by sequences targeting mRFP to the 3′ end of *DID2*. Recombinational repair of the break resulted in replacement of the entire *GFP-HISMX6* insertion with mRFP.

Various point mutant alleles of *VPS13* were introduced using the CRISPR/Cas9 strategy. The codon to be mutated was first replaced by the *HIS3MX6* cassette, and then cotransformation of pRS425-Cas9-*Sk*HIS3-381 with a 75-mer, single-stranded oligonucleotide carrying the mutated codon was performed. The exception was the *vps13-C89K* mutation, in which the rescue fragment was amplified by PCR from pRS426-*VPS13C89K* (plasmid construction described later). Transformants were screened for loss of the *HIS3* marker, and then the mutated region was amplified by PCR and sequenced to confirm the proper integration of the mutation. For strains JSP531, JSP533, JSP549, and JSP563 (*VPS13-G718K*), the starting strains were JSP499-1, RP301, BY4742, and JSP560, respectively. For strains RP201, RP202, RP203, and RP205 carrying disease alleles, the starting strain was BY4741. For strain RP301, the starting strain was AN117-16D.

Strains JSP536, JSP541, JSP545, JSP547, and JSP555 carrying *kanMX6*-marked deletions of *VPS13*, *NVJ1*, or *VAC8* were generated using flanking primers to amplify the deletion allele from genomic DNA of the appropriate strains in the yeast knockout collection (Winzeler *et al.*, 1999). The amplified knockout fragments were transformed into strains GCY3, GCY4, JSP497, and GCY1, transformants were selected on plates containing G418, and the knockouts were confirmed by colony PCR. Similarly, the C-terminal *GFP* fusion to *VPS13* was introduced into strain JSP549 by first amplifying the 3′ end of the *VPS13* gene, along with the *GFP* coding region and the *HIS3* selectable marker, from genomic DNA prepared from the *VPS13-GFPc* fusion in the yeast GFP-tagged collection (Huh *et al.*, 2003). Transformants were selected on synthetic defined medium (SD) –His plates and proper integration confirmed by PCR, generating strains JSP556 and JSP557.

JSP417 is a segregant from a cross of AN117-16D and HI27. JSP441, JSP442, and JSP443 are segregants from a cross between

Name	Genotype	Source
BY4741[a]	*MAT***a** *his3Δ0 leu2Δ0 met15Δ0 ura3Δ0 ho*	Winzeler *et al.* (1999)
BY4742[a]	*MATα his3Δ0 leu2Δ0 lys2Δ0 ura3Δ0 ho*	Winzeler *et al.* (1999)
JHY14[b,c,d]	*MATα lys2 ura3-52 leu2-3112 trp1-Δ1 mmm1-Δ1::LEU2 VPS13-G820D* [ρ^+, *TRP1*]	This study
JKY2[b]	*MATα lys2 ura3-52 leu2-3112 trp1-Δ1 vps13Δ::KAN-MX4* [ρ^+, *TRP1*]	This study
KWY70[b]	*MATα lys2 ura3-52 leu2-3112 trp1-Δ1 mmm1-Δ1::LEU2 VPS13-G820R* [ρ^+, *TRP1*]	This study
KWY75[b]	*MATα lys2 ura3-52 leu2-3112 trp1-Δ1 mmm1-Δ1::LEU2 VPS13-V1210E* [ρ^+, *TRP1*]	This study
KWY76[b]	*MATα lys2 ura3-52 leu2-3112 trp1-Δ1 mmm1-Δ1::LEU2 VPS13-N1467H* [ρ^+, *TRP1*]	This study
KWY80[b]	*MATα lys2 ura3-52 leu2-3112 trp1-Δ1 mmm1-Δ1::LEU2 VPS13-P268R* [ρ^+, *TRP1*]	This study
KWY105[b]	*MATα lys2 ura3-52 leu2-3112 trp1-Δ1 mmm1-Δ1::LEU2 VPS13-G1245S* [ρ^+, *TRP1*]	This study
KWY109[b]	*MATα lys2 ura3-52 leu2-3112 trp1-Δ1 mmm1-Δ1::LEU2 VPS13-G718K* [ρ^+, *TRP1*]	This study
KWY111[b]	*MATα lys2 ura3-52 leu2-3112 trp1-Δ1 mmm1-Δ1::LEU2 VPS13-L984S* [ρ^+, *TRP1*]	This study
KWY114[b]	*MATα lys2 ura3-52 leu2-3112 trp1-Δ1 mmm1-Δ1::LEU2 VPS13-A1512E* [ρ^+, *TRP1*]	This study
KWY131[b]	*MATα lys2 ura3-52 leu2-3112 trp1-Δ1 mmm1-Δ1::LEU2 VPS13-G718D* [ρ^+, *TRP1*]	This study
MTY71[b,c,d]	*MATα lys2 ura3-52 leu2-3112 trp1-Δ1 VPS13-L822F* [ρ^+, *TRP1*]	This study
MTY79[b,c,d]	*MATα lys2 ura3-52 leu2-3112 trp1-Δ1 mmm1-Δ1::LEU2 VPS13-L822F* [ρ^+, *TRP1*]	This study
PTY33[b]	*MAT***a** *ade2 ura3-52 leu2-3112 trp1-Δ1* [ρ^+, *TRP1*]	Thorsness and Fox (1993)
PTY44[b]	*MATα lys2 ura3-52 leu2-3112 trp1-Δ1* [ρ^+, *TRP1*]	Thorsness and Fox (1993)
PTY66[b,d]	*MATα lys2 ura3-52 leu2-3112 trp1-Δ1 vps13-31* [ρ^+, *TRP1*]	Thorsness and Fox (1993)
THY23[b]	*MATα lys2 ura3-52 leu2-3112 trp1-Δ1 mmm1-Δ1::LEU2* [ρ^o]	Hanekamp *et al.* (2002)
JSYD10	*MATα leu2 his3Δ MET15 ura3 arg4-NspI lys2 trp1::hisG ho* *MAT***a** *leu2Δ0 his3Δ0 met15Δ0 ura3Δ0 ARG4 LSY2 TRP1 ho* *mmm1Δ::kanMX6 VPS13* *MMM1 vps13-GFPc::HIS3MX6*	This study
GCY1[a]	*MAT***a** *his3Δ0 leu2Δ0 met15Δ0 ura3Δ0 ho vps13-GFPc::HIS3MX6*	Huh *et al.* (2003)
GCY2[a]	*MAT***a** *his3Δ0 leu2Δ0 met15Δ0 ura3Δ0 ho DID2::GFPc::HIS3MX6*	Huh *et al.* (2003)
GCY3[a]	*MAT***a** *his3Δ0 leu2Δ0 met15Δ0 ura3Δ0 ho NVJ1::GFP::HIS3MX6*	Huh *et al.* (2003)
GCY4[a]	*MAT***a** *his3Δ0 leu2Δ0 met15Δ0 ura3Δ0 ho VAC8::GFP::HIS3MX6*	Huh *et al.* (2003)
KO1[a]	*MAT***a** *his3Δ0 leu2Δ0 met15Δ0 ura3Δ ho vps13Δ::kanMX6 ho*	Winzeler *et al.* (1999)
KO3[a]	*MAT***a** *his3Δ0 leu2Δ0 met15Δ0 ura3Δ0 vps10Δ::kanMX6 ho*	Winzeler *et al.* (1999)
KO4[a]	*MAT***a** *his3Δ0 leu2Δ0 met15Δ0 ura3Δ0 ho mmm1Δ::kanMX6*/pRS316-*MMM1*	Winzeler *et al.* (1999)
KO5[a]	*MAT***a** *his3Δ0 leu2Δ0 met15Δ0 ura3Δ0 ho atg32Δ::kanMX6*	Winzeler *et al.* (1999)
JSP461-1[a]	*MAT***a** *his3Δ0 leu2Δ ura3Δ ho vps13Δ::HIS3MX6 atg32Δ::kanMX6*	This study
JSP497[a]	*MAT***a** *his3Δ0 leu2Δ0 met15Δ0 ura3Δ0 ho VPS13-GFP$_{1360}$*	This study
JSP513[a]	*MATα his3Δ0 leu2Δ0 lys2Δ0 ura3Δ0 ho GFP$_N$-vps13*	This study
RP201[a]	*MAT***a** *his3Δ0 leu2Δ0 met15Δ0 ura3Δ0 ho vps13-L66P*	This study
RP202[a]	*MAT***a** *his3Δ0 leu2Δ0 met15Δ0 ura3Δ0 ho vps13-L1107P*	This study
RP203[a]	*MAT***a** *his3Δ0 leu2Δ0 met15Δ0 ura3Δ0 ho vps13-Y2702C ho*	This study
RP205[a]	*MAT***a** *his3Δ0 leu2Δ0 met15Δ0 ura3Δ0 ho vps13-C89K*	This study
LUKE3[a]	*MAT***a** *his3Δ0 leu2Δ0 met15Δ0 ura3Δ0 ho VPS13-GFP$_{1360}$ mmm1Δ::kanMX6 ho*/pRS316-*MMM1*	This study
JSP499-1[a]	*MATα his3Δ0 leu2Δ0 lys2Δ0 ura3Δ0 ho VPS13-GFP$_{1360}$*	This study
JSP527[a]	*MATa leu2Δ0 his3Δ0 LYS2 met15Δ0 ura3Δ0 ho DID2::mRFP VPS13* *MATα leu2Δ0 his3Δ0 lys2Δ0 MET15 ura3Δ0 ho DID2 VPS13::GFP$_{1360}$*	This study

TABLE 3: Strains used in this study.

Continues

Name	Genotype	Source
JSP512[a]	*MAT***a** *his3Δ0 leu2Δ0 lys2Δ0 ura3Δ0 ho VPS13-GFP$_{1360}$ DID2::mRFP*	This study
JSP541[a]	*MAT***a** *his3Δ0 leu2Δ0 met15Δ0 ura3Δ0 ho VPS13-GFP$_{1360}$ nvj1Δ::kanMX6*	This study
JSP545[a]	*MAT***a** *his3Δ0 leu2Δ0 met15Δ0 ura3Δ0 ho VPS13-GFP$_{1360}$ vac8Δ::kanMX6*	This study
JSP547[a]	*MAT***a** *his3Δ0 leu2Δ0 met15Δ0 ura3Δ0 ho NVJ1::GFP::HIS3MX6 vac8Δ::kanMX6*	This study
JSP555[a]	*MAT***a** *his3Δ0 leu2Δ0 met15Δ0 ura3Δ0 ho VAC8::GFP::HIS3MX6 nvj1Δ::kanMX6*	This study
JSP495[a]	*MAT***a** *his3Δ0 leu2Δ0 met15Δ0 ura3Δ0 ho DID2::mRFP*	This study
JSP536[a]	*MAT***a** *his3Δ0 leu2Δ0 met15Δ0 ura3Δ0 ho vps13Δ::kanMX6 NVJ1::GFP::HIS3MX6*	This study
JSP531[a]	*MATα his3Δ0 leu2Δ0 lys2Δ0 ura3Δ0 ho VPS13-G718K-GFP$_{1360}$*	This study
JSP549[a]	*MATα his3Δ0 leu2Δ0 lys2Δ0 ura3Δ0 ho VPS13-G718K*	This study
JSP556[a]	*MATα his3Δ0 leu2Δ0 lys2Δ0 ura3Δ0 ho vps13-G718K-GFPc::HIS3MX6*	This study
JSP560[a]	*MAT***a** *his3Δ1 leu2Δ0 met 15Δ0 ura3Δ0 ho vps13-L66P-GFP$_{1360}$*	This study
JSP563[a]	*MAT***a** *his3Δ1 leu2Δ0 met 15Δ0 ura3Δ0 ho vps13-L66P G718K-GFP$_{1360}$*	This study
JSP590	*MAT***a** *his3Δ0 leu2Δ0 ura3Δ0 lys2Δ0 ho VPS13-G718K-GFPc::HIS3MX6 mmm1Δ::kanMX6/*pRS316-*MMM1*	This study
JSP577	*MAT***a** *his3 leu2 ura3 lys2 ho vps13-GFPc::HIS3MX6 mmm1Δ::kanMX6 /*pRS316-*MMM1*	This study
JSP442	*MATα his3Δ arg4-NspI leu2 lys2 trp1::hisG ura3 mmm1Δ::kanMX6*	This study
JSP443	*MAT***a** *leu2 trp1::hisG ura3 his3Δ ho vps13Δ::HIS3MX6 mmm1Δ::kanMX6 /*pRS316-*MMM1*	This study
JSP491	*MATα ura3 leu2 trp1::hisG his3Δ lys2 ho GFP$_N$-vps13 mmm1Δ::kanMX6*	This study
JSP552	*MAT***a** *his3 leu2 lys2 ura3 ho VPS13::GFP$_{1360}$ P$_{ADH1}$::NVJ1::3xmCherry::hphNT1*	This study
JSP446	*MATα his3 leu2 trp1::hisG ura3 ho vps13Δ::HIS3MX6 mmm1Δ::kanMX6 P$_{DIT1}$-lacZ::LEU2 /*pRS316-*MMM1*	This study
JSP582	*MAT***a** *his3 ura3 vps13-C89K mmm1Δ::kanMX6/* pRS316-*MMM1*	This study
JSP585	*MATα his3 leu2 ura3 trp1::hisG ho vps13-L1107P mmm1Δ::kanMX6 /*pRS316-*MMM1*	This study
RP301[e]	*MAT***a** *ura3 leu2 trp1-hisG his3Δ lys2 hoΔ::LYS2 VPS13-L66P mmm1Δ::kanMX6/* pRS316-*MMM1*	This study
JSP533[e]	*MAT***a** *ura3 leu2 trp1-hisG his3Δ lys2 ho::LYS2 vps13-L66P G718K mmm1Δ::kanMX6/*pRS316-*MMM1*	This study
JSP417[e]	*MATα his3ΔSK arg4-NspI leu2 ura3 trp1::hisG ho vps13Δ::HIS3MX6*	This study
JSP441	*MATα his3Δ leu2 trp1::hisG ura3 ho mmm1Δ::kanMX6 /*pRS316-*MMM1*	This study
JSP490[e]	*MAT***a** *ura3 leu2 trp1::hisG his3Δ lys2 ho::LYS2 GFP$_N$-vps13*	This study
CUY9002	*MATα leu2-3112 ura3-52 his3-Δ200 trp1-Δ101 lys2-801 suc2-Δ9 GAL natMX4-P$_{TEF1}$-GFP-VPS39 P$_{ADH}$1-NVJ1-3xmCherry-hphNT1*	Honscher *et al.* (2014)
HI27[e]	*MATα ura3 his3ΔSK trp1::hisG arg4-NspI lys2 hoΔ::LYS2 rme1::LEU2 leu2 vps13Δ::HIS3MX6 ho*	Nakanishi *et al.* (2007)
HI28[e]	*MAT***a** *ura3 his3ΔSK trp1::hisG lys2 hoΔ::LYS2 leu2 vps13Δ::HIS3MX6*	Nakanishi *et al.* (2007)
AN117-16D[e]	*MAT***a** *ura3 leu2 trp1::hisG his3ΔSK lys2 hoΔ::LYS2*	Neiman *et al.* (2000)
JSP528[e]	*MATa leu2 VPS13-GFP$_{1360}$ his3ΔSK arg4-NspI ura3 trp1::hisG lys2 ho:: LYS2* *MATα LEU2 VPS13-GFP$_{1360}$ his3ΔSK ARG4 ura3 trp1::hisG lys2 ho:: LYS2*	This study
JSYD1[f]	*MATa leu2Δ0 his3Δ0 met15Δ0 ura3Δ0 TRP1 ARG4 LYS2 ho* *MATα leu2 his3ΔSK MET15 ura3 trp1::hisG arg4-NspI lys2 hoΔ::LYS2* *RME1 VPS13* *rme1::LEU2 VPS13*	This study
JSYD2[f]	Same as JSYD1 only *vps13Δ::kanMX6* *vps13Δ::HIS3MX6*	This study
JSYD3[f]	Same as JSYD1 only *vps13-GFPc::HIS3MX6* *vps13Δ::HIS3MX6*	This study

TABLE 3: Strains used in this study.

Continues

Name	Genotype	Source
JSYD4[f]	Same as JSYD1 only *VPS13-GFP$_{1360}$* *vps13Δ::HIS3MX6*	This study
JSYD5[f]	Same as JSYD1 only *GFP$_N$-vps13* *vps13Δ::HIS3MX6*	This study
JSYD6[f]	Same as JSYD1 only *vps13-L66P* *vps13Δ::HIS3MX6*	This study
JSYD7[f]	Same as JSYD1 only *vps13-C89K* *vps13Δ::HIS3MX6*	This study
JSYD8[f]	Same as JSYD1 only *vps13-L1107P* *vps13Δ::HIS3MX6*	This study
JSYD9[f]	Same as JSYD1 only *vps13-Y2702C* *vps13Δ::HIS3MX6*	This study

[a]Isogenic with the BY4741 strain background.

[b]Strains are isogenic and were derived from D273-10B (Sherman, 1963).

[c]The mitochondrial genotype is bracketed.

[d]The *vps13-31* allele was previously designated *yme3-1* (Thorsness and Fox, 1993). The *VPS13-G820D* allele was previously designated *YNT61-1* (Hanekamp *et al.*, 2002). The *VPS13-L822F* allele had four previous designations; *YNT61-2*, *YNT61-3*, *YNT61-4*, and *YNT61-5* (Hanekamp *et al.*, 2002).

[e]Isogenic with the SK1 background.

[f]Strains are hybrids derived by crossing haploids from the BY4741 and SK1 background.

TABLE 3: Strains used in this study. Continued

JSP417 and KO4. JSP446 is a segregant from a cross between JSP441 and HI28 carrying P_{DIT1}-*lacZ::LEU2*. JSP491 is a segregant from a cross between JSP442 and JSP490. JSP552 is a segregant from a cross between CUY9002 and JSP497. JSP577 is a segregant from a cross between JSP441 and GCY1. JSP582 and JSP585 are segregants from crosses between JSP446 and RP205 or RP202, respectively. JSP590 is a segregant from a cross between JSP557 and KO4. JSP512 is a segregant from a cross between JSP495 and JSP499-1, and JSP527 was created by mating two segregants from this same cross.

Diploids JSYD1 to JSYD9 were generated as follows: BY4741 (*VPS13*) was mated to AN117-4B (*VPS13*) to create JSYD1. Haploids KO1 (*vps13Δ*), GCY1 (*vps13-GPF$_C$*), JSP497 (*VPS13-GFP-1360*), RP201 (*vps13-L66P*), RP205 (*vps13-C89K*), RP202 (*vps13-L1107P*), and RP203 (*vps13-Y2702C*) were crossed with HI27 (*vps13Δ*), resulting in JSYD2 to JSYD4 and JSYD6 to JSYD9, respectively. JSYD5 was generated by a cross of JSP513 (*GFP$_N$-vps13*) and HI28 (*vps13Δ*).

Suppressors of the *mmm1Δ* slow-growth phenotype were isolated from independent streaks of single colonies of THY23 (*mmm1Δ*) on rich-glucose medium. Initial isolates were colony purified by streaking three times onto rich-glucose medium. These isolates were then backcrossed to an isogenic wild type (PTY33), sporulated, and subjected to tetrad analysis. Strains JHY14, KWY70, KWY75, KWY76, KWY80, KWY105, KWY109, KWY111, KWY114, KWY131, and MTY79 are segregants from those crosses carrying both *mmm1Δ* and the suppressor mutation.

Plasmids

pRS426-*VPS13-C89K* was generated using site-directed mutagenesis. Briefly, a PCR fragment carrying the first 2345 base pairs of the *VPS13* coding region (*VPS13^{fragA}*) was cloned into the *Eco*RV site of pBluescript KS(+). Site-directed mutagenesis was performed in pBluescript KS(+)-*VPS13^{fragA}* using overlapping primers carrying the C89K (TGC-to-AAA) mutation, generating pBluescript KS(+)-*VPS13$^{fragA\text{-}C89K}$*. The mutation was confirmed by sequencing performed by the Stony Brook University DNA Sequencing Facility. pRS426-*VPS13-C89K* was finally constructed by homologous recombination of overlapping fragments of *VPS13$^{fragA\text{-}C89K}$* and other *VPS13* coding regions in *S. cerevisiae* as described in Park and Neiman (2012). Plasmid pRS316-*MMM1* was generated by subcloning a 2.1-kb *Bcl*I fragment of yeast genomic DNA containing *MMM1* into the *Bam*HI site of the *CEN/ARS/URA3* yeast shuttle vector, pRS316. This plasmid was previously given the name pRSMY6 (Hanekamp *et al.*, 2002). pVT100U-mtBFP was constructed by subcloning a *Hin*dIII-mtBFP-*Xho*I fragment from pYES-mtBFP (Westermann and Neupert, 2000) into *Hin*dIII/*Xho*I-digested expression vector pVT100U (Vernet *et al.*, 1987). Plasmids pBN-mtRosella and pRS426-R20 are described elsewhere (Bockler and Westermann, 2014).

Sporulation assays

Diploid cells were sporulated on Spo medium (2% agar, 1% potassium acetate, 0.05% yeast extract, and 0.05% glucose) at 30°C for 3–5 d. Three independent diploids from each cross were sporulated, and at least 200 cells were counted in each culture for the sporulation efficiency measurement.

For growth assay on plates, 3 µl of 10-fold serial dilutions were spotted onto yeast extract/peptone/glucose (YPD) rich medium and SD plus complete amino acids with 0.08% 5-FOA. These plates were incubated at 30°C until visible individual colonies were seen.

Western blot analysis

Exponentially growing cells (2 ml) were spun down to separate cell pellets containing internal cellular CPY and medium supernatants containing extracellular CPY. To prepare intracellular samples, cell pellets were resuspended in a solution of 100 µl of distilled water and 100 µl of 0.2 M NaOH and incubated for 5 min at room temperature. After pelleting the cells (6900 × *g*, 1 min), 50 µl of 1× SDS sample buffer (50 mM Tris-HCl, pH 6.8, 2% SDS, 10% glycerol, 0.1 mg/ml bromophenol blue, 0.36 M β-mercaptoethanol) was added to the pellets and the samples boiled for 5 min. To prepare the extracellular samples, 100% trichloroacetic acid (TCA) was added to the medium supernatants to a final concentration of 20% TCA. After 30 min of incubation on ice, the mixtures were centrifuged at

4°C at 16,000 × *g* for 15 min to precipitate proteins from the supernatants. The precipitants were washed with 300 µl of cold acetone and resuspended in 20 µl of 1× SDS sample buffer. Protein samples were fractionated using a 10% SDS-polyacrylamide gel, transferred to nitrocellulose, and probed with a 1:1000 dilution of monoclonal anti-CPY antibody (Life Technologies, Carlsbad, CA). The secondary antibody, horseradish peroxidase–conjugated sheep anti-mouse (GE Healthcare, Little Chalfont, UK), was used at a 1:2500 dilution, and the signal was detected using the ECL kit (Bio-Rad, Hercules, CA).

Mitophagy assay

Cells were grown overnight in either YPA or synthetic medium containing 2% galactose, 2% raffinose, and 0.1% glucose and lacking leucine to select for the mtRosella plasmid (pBN-mtRosella; Bockler and Westermann, 2014). Cells were washed with distilled water and diluted to a similar cell density of (1–2) × 10^6 cells/ml into either YPA from the YPA overnight culture or nitrogen starvation medium (0.17% yeast nitrogen base without amino acids and without ammonium sulfate; 2% glucose) from the synthetic medium overnight culture. The diluted cells were incubated at 30°C for 5.5 h and then examined by fluorescence microscopy.

Microscopy

Live-cell imaging was performed using either a Zeiss Axioplan2 microscope (Carl Zeiss, Thornwood, NY) with a Zeiss mRM AxioCam or a Zeiss Observer.Z1 microscope with an attached Orca II ERG camera (Hamamatsu, Bridgewater, NJ). Zeiss AxioVision 4.8 and ZEN 2012 (Blue edition) software were used to acquire images.

To visualize the vacuolar membrane, vacuolar lumen, and nucleus in live cells, FM4-64, blue CMAC, and Hoechst 33342 (all obtained from ThermoFisher, Waltham, MA) were used, respectively. FM4-64 was added for a final concentration of 2 µg/ml in live cells and incubated at 30°C for 1 h. Hoechst was then added to a final concentration of 3.3 µM, and the cells were incubated for an additional 10 min. Cells stained with FM4-64 and Hoechst were washed once in phosphate-buffered saline and observed by fluorescence microscopy. Blue CMAC was added to a final concentration of 100 µM to live cells and incubated at room temperature for 15–30 min. Cells were then washed once in fresh medium and observed by fluorescence microscopy.

To quantify the colocalization of Vps13-GFP_{1360} and endosomes, strains JSP512 and JSP527, expressing both Vps13-GFP_{1360} and Did2-mRFP were examined The percentage colocalization was defined as the fraction of GFP foci displaying overlap with RFP as defined by the presence of yellow (mixed red/green) signal. The percentage reported is the average of four independent experiments with at least 100 GFP foci counted in each experiment. The frequency of Vps13-GFP_{1360} localization at endosome–mitochondrial junctions was determined in JSP512/pVT100-mtBFP possessing all three markers (*VPS13-*GFP_{1360}, *DID2-mRFP*, and *mtBFP*). The GFP foci overlapping with mRFP foci were first identified as described, and the fraction of these foci that also overlapped with the mitochondrial BFP signal was determined. The percentage reported is the average of two independent experiments with 200 GFP foci scored in both experiments.

ACKNOWLEDGMENTS

We thank members of the Stony Brook Yeast Center for helpful discussions. This work was supported by National Institutes of Health Grants R01 GM072540 to A.M.N. and R01 GM050717 to N.M.H.

REFERENCES

Bankaitis VA, Johnson LM, Emr SD (1986). Isolation of yeast mutants defective in protein targeting to the vacuole. Proc Natl Acad Sci USA 83, 9075–9079.

Bockler S, Westermann B (2014). Mitochondrial ER contacts are crucial for mitophagy in yeast. Dev Cell 28, 450–458.

Boeke JD, Trueheart J, Natsoulis G, Fink GR (1987). 5-Fluoroorotic acid as a selective agent in yeast molecular genetics. Methods Enzymol 154, 164–175.

Brickner JH, Fuller RS (1997). *SOI1* encodes a novel, conserved protein that promotes TGN-endosomal cycling of Kex2p and other membrane proteins by modulating the function of two TGN localization signals. J Cell Biol 139, 23–36.

Burte F, Carelli V, Chinnery PF, Yu-Wai-Man P (2015). Disturbed mitochondrial dynamics and neurodegenerative disorders. Nat Rev Neurol 11, 11–24.

Campbell CL, Thorsness PE (1998). Escape of mitochondrial DNA to the nucleus in *yme1* yeast is mediated by vacuolar-dependent turnover of abnormal mitochondrial compartments. J Cell Sci 111, 2455–2464.

Costanzo M, Baryshnikova A, Bellay J, Kim Y, Spear ED, Sevier CS, Ding H, Koh JL, Toufighi K, Mostafavi S, *et al*. (2010). The genetic landscape of a cell. Science 327, 425–431.

Dobson-Stone C, Danek A, Rampoldi L, Hardie RJ, Chalmers RM, Wood NW, Bohlega S, Dotti MT, Federico A, Shizuka M, *et al*. (2002). Mutational spectrum of the *CHAC* gene in patients with chorea-acanthocytosis. Eur J Hum Genet 10, 773–781.

Elbaz-Alon Y, Eisenberg-Bord M, Shinder V, Stiller SB, Shimoni E, Wiedemann N, Geiger T, Schuldiner M (2015). Lam6 regulates the extent of contacts between organelles. Cell Rep 12, 7–14.

Elbaz-Alon Y, Rosenfeld-Gur E, Shinder V, Futerman AH, Geiger T, Schuldiner M (2014). A dynamic interface between vacuoles and mitochondria in yeast. Dev Cell 30, 95–102.

Enyenihi AH, Saunders WS (2003). Large-scale functional genomic analysis of sporulation and meiosis in *Saccharomyces cerevisiae*. Genetics 163, 47–54.

Hanekamp T, Thorsness MK, Rebbapragada I, Fisher EM, Seebart C, Darland MR, Coxbill JA, Updike DL, Thorsness PE (2002). Maintenance of mitochondrial morphology is linked to maintenance of the mitochondrial genome in *Saccharomyces cerevisiae*. Genetics 162, 1147–1156.

Hayashi T, Kishida M, Nishizawa Y, Iijima M, Koriyama C, Nakamura M, Sano A, Kishida S (2012). Subcellular localization and putative role of VPS13A/chorein in dopaminergic neuronal cells. Biochem Biophys Res Commun 419, 511–516.

Helle SC, Kanfer G, Kolar K, Lang A, Michel AH, Kornmann B (2013). Organization and function of membrane contact sites. Biochim Biophys Acta 1833, 2526–2541.

Henne WM, Liou J, Emr SD (2015). Molecular mechanisms of inter-organelle ER-PM contact sites. Curr Opin Cell Biol 35, 123–130.

Hobbs AE, Srinivasan M, McCaffery JM, Jensen RE (2001). Mmm1p, a mitochondrial outer membrane protein, is connected to mitochondrial DNA (mtDNA) nucleoids and required for mtDNA stability. J Cell Biol 152, 401–410.

Honscher C, Mari M, Auffarth K, Bohnert M, Griffith J, Geerts W, van der Laan M, Cabrera M, Reggiori F, Ungermann C (2014). Cellular metabolism regulates contact sites between vacuoles and mitochondria. Dev Cell 30, 86–94.

Hoppins S, Collins SR, Cassidy-Stone A, Hummel E, Devay RM, Lackner LL, Westermann B, Schuldiner M, Weissman JS, Nunnari J (2011). A mitochondrial-focused genetic interaction map reveals a scaffold-like complex required for inner membrane organization in mitochondria. J Cell Biol 195, 323–340.

Huh WK, Falvo JV, Gerke LC, Carroll AS, Howson RW, Weissman JS, O'Shea EK (2003). Global analysis of protein localization in budding yeast. Nature 425, 686–691.

Jin L, Zhang K, Xu Y, Sternglanz R, Neiman AM (2015). Sequestration of mRNAs modulates the timing of translation during meiosis in budding yeast. Mol Cell Biol 35, 3448–3458.

Kanki T, Wang K, Cao Y, Baba M, Klionsky DJ (2009). Atg32 is a mitochondrial protein that confers selectivity during mitophagy. Dev Cell 17, 98–109.

Kolehmainen J, Black GC, Saarinen A, Chandler K, Clayton-Smith J, Traskelin AL, Perveen R, Kivitie-Kallio S, Norio R, Warburg M, *et al*. (2003). Cohen syndrome is caused by mutations in a novel gene, *COH1*, encoding a transmembrane protein with a presumed role in vesicle-mediated sorting and intracellular protein transport. Am J Hum Genet 72, 1359–1369.

Kornmann B, Walter P (2010). ERMES-mediated ER-mitochondria contacts: molecular hubs for the regulation of mitochondrial biology. J Cell Sci 123, 1389–1393.
Krols M, van Isterdael G, Asselbergh B, Kremer A, Lippens S, Timmerman V, Janssens S (2016). Mitochondria-associated membranes as hubs for neurodegeneration. Acta Neuropathol 505–523.
Kurano Y, Nakamura M, Ichiba M, Matsuda M, Mizuno E, Kato M, Agemura A, Izumo S, Sano A (2007). In vivo distribution and localization of chorein. Biochem Biophys Res Commun 353, 431–435.
Kvam E, Gable K, Dunn TM, Goldfarb DS (2005). Targeting of Tsc13p to nucleus-vacuole junctions: a role for very-long-chain fatty acids in the biogenesis of microautophagic vesicles. Mol Biol Cell 16, 3987–3998.
Kvam E, Goldfarb DS (2004). Nvj1p is the outer-nuclear-membrane receptor for oxysterol-binding protein homolog Osh1p in *Saccharomyces cerevisiae*. J Cell Sci 117, 4959–4968.
Lang AB, John Peter AT, Walter P, Kornmann B (2015). ER-mitochondrial junctions can be bypassed by dominant mutations in the endosomal protein Vps13. J Cell Biol 210, 883–890.
Lesage S, Drouet V, Majounie E, Deramecourt V, Jacoupy M, Nicolas A, Cormier-Dequaire F, Hassoun SM, Pujol C, Ciura S, *et al*. (2016). Loss of *VPS13C* function in autosomal-recessive parkinsonism causes mitochondrial dysfunction and increases PINK1/Parkin-dependent mitophagy. Am J Hum Genet 98, 500–513.
Longtine MS, McKenzie A 3rd, Demarini DJ, Shah NG, Wach A, Brachat A, Philippsen P, Pringle JR (1998). Additional modules for versatile and economical PCR-based gene deletion and modification in *Saccharomyces cerevisiae*. Yeast 14, 953–961.
Lottridge JM, Flannery AR, Vincelli JL, Stevens TH (2006). Vta1p and Vps46p regulate the membrane association and ATPase activity of Vps4p at the yeast multivesicular body. Proc Natl Acad Sci USA 103, 6202–6207.
Mijaljica D, Prescott M, Devenish RJ (2011). A fluorescence microscopy assay for monitoring mitophagy in the yeast *Saccharomyces cerevisiae*. J Vis Exp pii 2779.
Murley A, Sarsam RD, Toulmay A, Yamada J, Prinz WA, Nunnari J (2015). Ltc1 is an ER-localized sterol transporter and a component of ER-mitochondria and ER-vacuole contacts. J Cell Biol 209, 539–548.
Nakanishi H, Suda Y, Neiman AM (2007). Erv14 family cargo receptors are necessary for ER exit during sporulation in *Saccharomyces cerevisiae*. J Cell Sci 120, 908–916.
Neiman AM (2011). Sporulation in the budding yeast *Saccharomyces cerevisiae*. Genetics 189, 737–765.
Neiman AM, Katz L, Brennwald PJ (2000). Identification of domains required for developmentally regulated SNARE function in *Saccharomyces cerevisiae*. Genetics 155, 1643–1655.
Okamoto K, Kondo-Okamoto N, Ohsumi Y (2009). Mitochondria-anchored receptor Atg32 mediates degradation of mitochondria via selective autophagy. Dev Cell 17, 87–97.
Olkkonen VM (2015). OSBP-related protein family in lipid transport over membrane contact sites. Lipid Insights 8, 1–9.
Pan X, Roberts P, Chen Y, Kvam E, Shulga N, Huang K, Lemmon S, Goldfarb DS (2000). Nucleus-vacuole junctions in *Saccharomyces cerevisiae* are formed through the direct interaction of Vac8p with Nvj1p. Mol Biol Cell 11, 2445–2457.
Park JS, Halegoua S, Kishida S, Neiman AM (2015). A conserved function in phosphatidylinositol metabolism for mammalian Vps13 family proteins. PLoS One 10, e0124836.
Park JS, Neiman AM (2012). *VPS13* regulates membrane morphogenesis during sporulation in *Saccharomyces cerevisiae*. J Cell Sci 125, 3004–3011.
Park JS, Okumura Y, Tachikawa H, Neiman AM (2013). *SPO71* encodes a developmental stage-specific partner for *VPS13* in *Saccharomcyes cerevisiae*. Eukaryot Cell 12, 1530–1537.
Raiborg C, Wenzel EM, Stenmark H (2015). ER-endosome contact sites: molecular compositions and functions. EMBO J 34, 1848–1858.
Rampoldi L, Dobson-Stone C, Rubio JP, Danek A, Chalmers RM, Wood NW, Verellen C, Ferrer X, Malandrini A, Fabrizi GM, *et al*. (2001). A conserved sorting-associated protein is mutant in chorea-acanthocytosis. Nat Genet 28, 119–120.
Rosado CJ, Mijaljica D, Hatzinisiriou I, Prescott M, Devenish RJ (2008). Rosella: a fluorescent pH-biosensor for reporting vacuolar turnover of cytosol and organelles in yeast. Autophagy 4, 205–213.
Rose MD, Fink GR (1990). Methods in Yeast Genetics, Cold Spring Harbor, NY: Cold Spring Harbor Laboratory Press.
Schrader M, Godinho LF, Costello JL, Islinger M (2015). The different facets of organelle interplay-an overview of organelle interactions. Front Cell Dev Biol 3, 56.
Sherman F (1963). Respiration-deficient mutants of yeast. I. Genetics. Genetics 48, 375–385.
Stefan CJ, Blumer KJ (1999). A syntaxin homolog encoded by *VAM3* mediates down-regulation of a yeast G protein-coupled receptor. J Biol Chem 274, 1835–1841.
Suda Y, Nakanishi H, Mathieson EM, Neiman AM (2007). Alternative modes of organellar segregation during sporulation in *Saccharomyces cerevisiae*. Eukaryot Cell 6, 2009–2017.
Thorsness PE, Fox TD (1993). Nuclear mutations in *Saccharomyces cerevisiae* that affect the escape of DNA from mitochondria to the nucleus. Genetics 134, 21–28.
Tomiyasu A, Nakamura M, Ichiba M, Ueno S, Saiki S, Morimoto M, Kobal J, Kageyama Y, Inui T, Wakabayashi K, *et al*. (2011). Novel pathogenic mutations and copy number variations in the VPS13A gene in patients with chorea-acanthocytosis. Am J Med Genet B Neuropsychiatr Genet 156B, 620–631.
Toulmay A, Prinz WA (2011). Lipid transfer and signaling at organelle contact sites: the tip of the iceberg. Curr Opin Cell Biol 23, 458–463.
Ueno S, Maruki Y, Nakamura M, Tomemori Y, Kamae K, Tanabe H, Yamashita Y, Matsuda S, Kaneko S, Sano A (2001). The gene encoding a newly discovered protein, chorein, is mutated in chorea-acanthocytosis. Nat Genet 28, 121–122.
Velayos-Baeza A, Vettori A, Copley RR, Dobson-Stone C, Monaco AP (2004). Analysis of the human *VPS13* gene family. Genomics 84, 536–549.
Vernet T, Dignard D, Thomas DY (1987). A family of yeast expression vectors containing the phage f1 intergenic region. Gene 52, 225–233.
Westermann B, Neupert W (2000). Mitochondria-targeted green fluorescent proteins: convenient tools for the study of organelle biogenesis in *Saccharomyces cerevisiae*. Yeast 16, 1421–1427.
Winzeler EA, Shoemaker DD, Astromoff A, Liang H, Anderson K, Andre B, Bangham R, Benito R, Boeke JD, Bussey H, *et al*. (1999). Functional characterization of the *S. cerevisiae* genome by gene deletion and parallel analysis. Science 285, 901–906.